July 23, 2018

SURF: Understanding and Predicting Urban Convection and Haze

X. Liang, *China Meteorological Administration*
S. Miao, *China Meteorological Administration*
J. Li, *China Meteorological Administration*
R. Bornstein, *China Meteorological Administration*
X. Zhang, *Chengdu University of Information Technology*, et al.

SURF

Understanding and Predicting Urban Convection and Haze

X. Liang, S. Miao, J. Li, R. Bornstein, X. Zhang, Y. Gao, F. Chen, X. Cao, Z. Cheng, C. Clements, W. Dabberdt, A. Ding, D. Ding, J. J. Dou, J. X. Dou, Y. Dou, C. S. B. Grimmond, J. E. González-Cruz, J. He, M. Huang, X. Huang, S. Ju, Q. Li, D. Niyogi, J. Quan, J. Sun, J. Z. Sun, M. Yu, J. Zhang, Y. Zhang, X. Zhao, Z. Zheng, and M. Zhou

Comprehensive multiscale observations and modeling are enabling an international team of scientists to understand and better predict urban effects on heavy summertime convective precipitation and wintertime fine-particle pollutant episodes in the greater Beijing metropolitan area.

The order is rapidly fadin'.
And the first one now will later be last
For the times they are a-changin'.
—Bob Dylan[1]

Global urbanization has accelerated over the past 65 years; in 1950, 30% (746 million people) of the global population resided in cities, but by 2014, that number had increased to 54% (3.9 billion), and the United Nations projects a value of 66% (6.4 billion) by 2050 (United Nations 2014). Half of all urbanites currently live in small cities, while 28 megacities (>10 million) already have 13% of the global population; by 2030, 41 megacities will exist. Urbanization challenges society and science; overcrowding, infrastructure, and economic activities make cities vulnerable to disasters like flooding and haze, according to a United Nations (2016a) report.

The High Impact Weather Program of the World Meteorological Organization (WMO; WMO 2013) lists urban-induced floods as well as heat waves and air pollution as three of its five major foci. In the United States, urban heat waves produce more weather-related deaths than any other weather phenomenon (National Research Council 2010). More than 700 deaths occurred from a 1995 five-day Chicago heat wave, while a 2015 event in India resulted in nearly 2,500 deaths (Di Liberto 2015). The 14-day European August 2003 heat wave claimed 40,000 lives (Robine et al. 2007), with a large number in cities (Vandentorren et al. 2004). Heavy rainfall caused flooding in July 2012, killing 79 people in Beijing, China, and with losses of $1.7 billion (U.S. dollars).

Urban areas also enhance the severity of gaseous and (solid and liquid) aerosol pollution, producing photochemical haze, smog, and acid rain episodes (Cao et al. 2013). One billion people experience excessive outdoor pollution, and during 2012, air pollution was linked to one of every eight deaths globally (United Nations 2016b). Urban air pollution costs approximately 2% of GDP in developed countries and 5% in developing countries.

Anthropogenic aerosols penetrate deep into human organs (Li et al. 2011) and cause severe health consequences (e.g., asthma, heart attacks, nervous

[1] From "The Times They Are a-Changin'," ©1963, 1964 by Warner Bros., Inc.; renewed 1991, 1992 by Special Rider Music.

system damage, and lung cancer; Tie et al. 2009). Aerosol impacts on weather and climate include alterations of radiation fluxes (Andreae et al. 2005), horizontal visibility (Quan et al. 2015), atmospheric stability (Zhao et al. 2006), planetary boundary layer (PBL) development (Quan et al. 2013), cloud formation (Andreae et al. 2004), and convective precipitation (Rosenfeld et al. 2008). While significant knowledge concerning aerosol impacts on some aspects of weather systems has been obtained, their impacts on radiation (Ao et al. 2016; Wang et al. 2016), clouds, and rainfall is far from complete, especially in urban areas (Stevens 2008).

Observation and numerical modeling are two important methods used in urban weather studies. Concurrent observations of processes in adjacent urban and rural atmospheres are fundamental to understanding interactions between underlying surfaces, aerosols, and the atmosphere. Numerical models for urban weather and air quality provide valuable information to decision-makers and the public for many applications. The WMO has proposed that National Meteorological and Hydrological Services produce impact-based forecasts for environmental, energy, transportation, and health effects (Tan et al. 2015). Urban forecast model skill should increase as a better understanding of urban atmospheric processes emerges from large field measurement programs (Shepherd 2005).

URBAN THUNDERSTORMS. Urban impacts on precipitation were the focus of the now-classic 1970s Metropolitan Meteorological Experiment (METROMEX) field study (FS), which investigated modification of summer convective rainfall by the St. Louis, Missouri, urban area. Observations showed that the urban area increased precipitation, both within the city and 50–75 km downwind of it, by 5%–25% over upwind values (Huff and Vogel 1978; Changnon 1979; Changnon et al. 1981; Braham et al. 1981; Changnon et al. 1991). Similar results were found by Shepherd et al. (2002) around Atlanta, Georgia, and four other large U.S. cities (Burian and Shepherd 2005).

Radar images of 91 summer thunderstorms during 2000–09 over Indianapolis, Indiana, by Niyogi et al. (2011), however, showed 60% of them with a variety of alterations (i.e., they initiated, intensified, split, or dissipated) over the city. These results agreed with the older observations by Bornstein and LeRoy (1990) for New York City (NYC), and Bornstein and Lin (2000) for Atlanta, as both studies also showed both urban-initiated and urban-bifurcated (i.e., splitting and going around the city, respectively) thunderstorms.

Numerical modeling enables controlled experiments to characterize physical processes producing urban precipitation modification. Fifth-generation Pennsylvania State University–National Center for Atmospheric Research Mesoscale Model (MM5) simulations by Craig and Bornstein (2002) showed an Atlanta thunderstorm arising from urban heat island (UHI)-induced convergence over the city. Simulations of two thunderstorms over Atlanta with the Weather Research and Forecasting (WRF) Model by Shem and Shepherd (2009) also showed the convergence effect, with rainfall increases downwind of the city. A case simulation with WRF and its single-layer urban canopy model (SLUCM) option by Miao et al. (2011) showed that early (prior to 1980) Beijing urbanization decreased (as compared with a no-urban simulation) maximum rainfall over Beijing because of increased urban surface dryness. Further

AFFILIATIONS: Liang,* Miao, J. Li, Cao, Cheng, J. J. Dou, J. X. Dou, Y. Dou, He, M. Huang, Ju, Q. Li, Quan, Yu, J. Zhang, Y. Zhang, Zhao, and Zheng—Institute of Urban Meteorology, China Meteorological Administration, Beijing, China; Bornstein—Institute of Urban Meteorology, China Meteorological Administration, Beijing, China, and San Jose State University, San Jose, California; X. Zhang—School of Atmospheric Sciences, Plateau Atmosphere and Environment Key Laboratory of Sichuan Province, Chengdu University of Information Technology, Chengdu, China, and Environmental Meteorology Forecast Center of Beijing–Tianjin–Hebei, Beijing; Gao and D. Ding—Beijing Weather Modification Office, Beijing, China; Chen, J. Sun, and J. Z. Sun—National Center for Atmospheric Research, Boulder, Colorado; Clements—San Jose State University, San Jose, California; Dabberdt—Vaisala Group, Boulder, Colorado; A. Ding and X. Huang—Nanjing University, Nanjing, China; Grimmond—University of Reading, Reading, United Kingdom; González-Cruz—City College of the City University of New York, New York, New York; Niyogi—Purdue University, West Lafayette, Indiana; Zhou—National Marine Environment Forecast Center, Beijing, China
***CURRENT AFFILIATION:** State Key Laboratory of Severe Weather, Chinese Academy of Meteorological Sciences, Beijing, China
CORRESPONDING AUTHOR: Shiguang Miao, sgmiao@ium.cn

The abstract for this article can be found in this issue, following the table of contents.
DOI:10.1175/BAMS-D-16-0178.1

A supplement to this article is available online (10.1175/BAMS-D-16-0178.2).

In final form 15 January 2018

urbanization decreased rainfall, however, as storms bifurcated around the city.

A case study WRF simulation, coupled with its multilevel Building Environment Parameterization (BEP) urbanization option, by Yu and Liu (2015) showed that Beijing produced upstream and downstream precipitation increases. Yu et al. (2017) used SLUCM to simulate a heavy August Beijing storm, and results showed suburban increases of sensible heat flux, temperature, and wind speed, which facilitated storm merging and enhanced precipitation. Zhang et al. (2017b) simulated two Beijing summer thunderstorms with SLUCM and showed contrasting urban effects on precipitation under strong and weak UHIs (i.e., initiation vs bifurcation, respectively).

Recent reviews have summarized the processes producing urban impacts on precipitation; for example, Shepherd (2005) reviewed publications from 1990 to 2005, covering observations and simulations and stressing both thermodynamic and microphysical impacts. Shepherd (2013) reviewed post-METROMEX lightning and winter precipitation studies, focusing on fluxes, aerosols, and bifurcation. Han et al. (2014) stressed a range of urban precipitation enhancers, from UHIs to surface roughness to aerosols, while Mitra and Shepherd (2016) focused on resulting storm modifications (e.g., bifurcation, merging).

To address the above "apparently conflicting" urban precipitation impacts in the literature, a synthesis–hypothesis was proposed by Bornstein (2011) in which strong UHIs initiate convective activity (and thus produce a city-center precipitation maximum) during periods with near-calm regional flows. During strong wind, weak UHI conditions, however, moving thunderstorms bifurcate and move around cities because of building-barrier effects. This latter effect thus produces a precipitation minimum over and downwind of cities and maximum around the city in lateral boundary convergence zones and in the downwind reconvergence area.

Dou et al. (2015) for the first time showed UHI magnitude as key to determining urban effects on summer thunderstorms. Based on 2008–12 Beijing hourly precipitation observations, they showed that strong (greater than average) UHIs induced or enhanced thunderstorm formation. With weak UHI conditions, however, thunderstorms bifurcated and bypassed the city because of building-barrier effects. This study was thus the first validation of the Bornstein (2011) hypothesis concerning how UHI magnitude impacts summer convective precipitation, but an analysis of simulation results to understand bifurcation dynamics is still lacking.

Numerical modeling of urban thunderstorms relies heavily on numerical weather prediction simulation results to provide background conditions. Such models, however, still have significant uncertainties in the estimation of the timing and amount of precipitation. Uncertainties in the numerical simulation of urbanization impacts on heavy rainfall, in particular, thus still require further investigation (Yu et al. 2018, manuscript submitted to *J. Geophys. Res. Atmos.*).

URBAN AEROSOLS AND HAZE. Atmospheric aerosols, also called particulate matter (PM), directly influence radiation transfer processes and cause direct climate effects because of their optical scattering and absorption properties (Charlson et al. 1992). As cloud condensation nuclei (CCN), they indirectly influence climate by changing cloud formation, precipitation, and radiation transfer processes (Rosenfeld et al. 2007; Liu and Daum 2002). Atmospheric aerosols have a variety of sources, as well as complex chemical compositions and physical properties, with anthropogenic fossil fuel combustion as their largest source (Andreae and Crutzen 1997). Biomass burning, windblown dust, sea salt, and volcanoes are other important global sources. Chemical composition affects radiative transfer and cloud formation processes; for example, black carbon (also called soot) and dust are the two most important absorption aerosols (Bond et al. 2013), while important scattering aerosols include sulfates, nitrates, and ammonium.

Aerosol impacts on cloud microphysical processes, (e.g., evaporation, condensation, collision and coalescence, and droplet breakup) are better understood on larger scales than for city scales (van den Heever and Cotton 2007). Generalization of natural aerosol impacts is difficult, however, as they range from precipitation enhancement to suppression; for example, high concentrations in winter orographic clouds yield more cloud water but less rainwater (Rosenfeld et al. 2008). Too many CCN reduce autoconversion rates, since droplets coalesce less efficiently than giant CCN (GCCN), such as sea salts (Grabowski 1999). When droplets ascend above the freezing level, precipitation enhancement results, however, by dynamic invigoration from frozen droplets (Carrió et al. 2010), forming hail and graupel. An excellent review of all aspects of these processes appears in Fan et al. (2016). Biomass smoke also significantly alters synoptic weather (Robock 1991), and fossil fuel aerosols alter regional (or even global) climates (Jacobson 2001).

Urban environments, with abundant pollutant CCN and GCCN, thus also modify cloud microphysical processes (after dynamical effects initiate it, as discussed above). Pollution aerosols have resulted in annual precipitation losses of 15%–25% over topographic barriers downwind of major coastal urban areas in California and Israel (Givati and Rosenfeld 2004). Aerosol particle size distribution (PSD) also affects microphysical processes; for example, Regional Atmospheric Modeling System (RAMS) idealized simulations by Comarazamy et al. (2006) for Puerto Rico showed that cloud droplet production is significantly larger in polluted air than in clear skies and that rainwater in polluted air is less than that in unpolluted air. Building from this study, Hosannah and Gonzalez (2014) simulated impacts on a local NYC thunderstorm event by ingestion of observed Aerosol Robotic Network (AERONET) PSDs (https://aeronet.gsfc.nasa.gov/). Results showed impacted precipitation totals, rates, and spatial patterns, while monthlong simulations showed smaller prediction errors with observed PSDs than with assumed model distributions.

As one of the most densely populated countries, China has high aerosol loadings because of intense anthropogenic and natural emissions. Its complex aerosol sources and geographical distribution, together with the large-scale circulations of the East Asian monsoons, cause a complex transport and mixing of air masses, producing strong chemical and physical interactions (Ding et al. 2016). Long-term multisatellite observations of rainfall, clouds, and aerosols indicate that they influence cloud properties, particularly cloud droplet size (Jin and Shepherd 2008).

Beijing is one of the largest cities in China, with a population over 20 million, and it suffers from high aerosol concentrations and, with its nearby complex terrain, is an excellent region to study aerosol–cloud–precipitation interactions. Many observational and numerical studies have investigated the role of aerosol on its radiation balance and precipitation processes. Surface radiation observations by Wang et al. (2016) at four Beijing sites showed polluted days having both attenuated direct and downward-scattered shortwave (SW) radiation fluxes. Modeling by Chen et al. (2015) found that while aerosols decreased Beijing urban-area rainfall, they increased domain-averaged values. Zhong et al. (2015) compared impacts from UHIs and aerosols on a summer precipitation event over Beijing with a WRF coupled with chemistry (WRF-Chem)–urban canopy model (UCM) ensemble. Results showed aerosol impacts dominant, with enhanced downstream convection and precipitation.

Direct observational evidence on the relationship between aerosols and cloud/precipitation in Beijing is still limited, however, thus requiring time-resolving measurements of both aerosols and weather processes. The Study of Urban Impacts on Rainfall and Fog/Haze (SURF) project, which includes radiometer, lidar, radar, tower, and aircraft measurements, was

PROGRAM SYNOPSIS

The SURF project investigates urban, terrain, convection, and aerosol interactions for improved weather and air quality forecast accuracy achieved by the combination of expertise from an international group of multidisciplinary scientists and by the employment of complementary research methodologies. Principal Chinese participants were from the IUM, Environmental Meteorology Forecast Center (EMFC), Chengdu University of Information Technology (CUIT), BJWMO, and National Marine Environment Forecast Center (NMERC). Principal international groups include San Jose State University (SJSU), National Center for Atmospheric Research (NCAR), Vaisala Group (VG), University of Reading (UR), City College of New York (CCNY), and Purdue University (PU).

SURF consists of four symbiotic components:

- Observations with research-level BL instrumentation to augment extensive operational surface, BL, and upper-air networks during SURF summer thunderstorm and winter haze field study periods. Resulting data are archived, quality controlled, and available to Chinese and international partners.
- Numerical model development and verification activities, which involved use of SURF observations to develop and test advanced modules to improve urban parameterizations in the operational and research-grade urbanized WRF Model (Skamarock et al. 2008) and in air quality models. New parameterizations are available for inclusion in publically available versions of the WRF Model.
- Modeling of case studies that involves use of the newly upgraded research-grade weather and air quality numerical models to simulate SURF golden-case thunderstorms and haze events, whose model input and output data are available to interested modelers.
- Applications with the newly upgraded operational numerical models for improved IUM urban weather and air quality forecasts and for use by health, energy, hydrologic, climate change, air quality, planning, and emergency response managers.

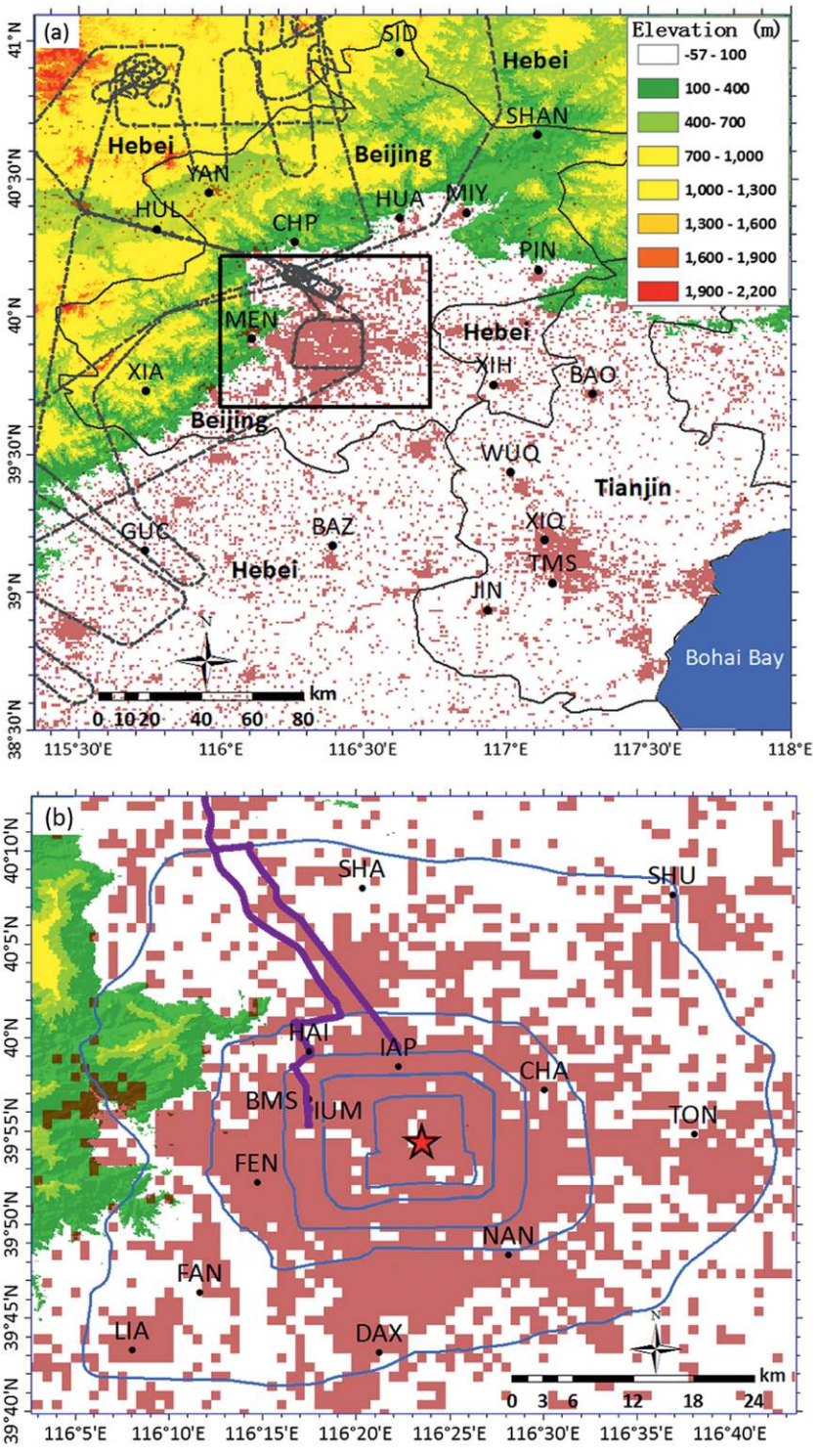

Fig. 1. Study area (a) full and (b) Beijing zoom-in [area of black box in (a)]; with topography (m; color bar); urban areas (pink); province names (full words); Tiananmen Square (red star); PBL instrument sites (dots; abbreviations defined in Table ES1); King Air flight tracks (dashes); mobile lidar route (purple), which starts from IAP and ends at IUM; and Beijing ring roads 2 to 6 (light blue circles).

thus initialized in 2015 to study aerosol effects on Beijing haze and precipitation processes.

CRITICAL SCIENCE NEEDS. The Beijing–Tianjin–Hebei (BTH) area (Fig. 1a) includes the megacities of Beijing, Tianjin, Shijiazhuang, and Tangshan, China, with 90 million people, with 40 million just in the Beijing–Langfang–Tianjin belt. The BTH area includes complex topography with mountains, plains, and coastal areas (Fig. 1a), and 7 of the 10 most polluted Chinese cities, with 40% of days during 2013 (mostly in winter) having "very hazardous" air quality (China Ministry of Environmental Protection 2014).

Severe spring pollution frequently impacts Beijing and northern China, with hourly PM_{10} concentrations as high as 1,000 $\mu g\ m^{-3}$. Regional transport by summer monsoons subjects Beijing and surrounding cities to high concentrations of secondary aerosols from the north China plain and southern China (Wang et al. 2010). Severe autumn and winter haze events also occur in Beijing; for example, $PM_{2.5}$ concentrations were >800 $\mu g\ m^{-3}$ in January 2013 (Guo et al. 2014). Such episodes occur under stagnant, weak synoptic conditions, especially one or two days before a cold front passage. During haze episodes, the sky is colored light yellow or orange-gray and has a pungent smell.

Given the human and environmental tolls from Beijing haze and floods (resulting from the precipitation processes discussed above), the Chinese Ministry of Science and Technology provided support to the Institute of Urban Meteorology (IUM) for extensive field measurement and modeling campaigns to study both Beijing summer convective thunderstorm

and winter haze events. A preliminary workshop (March 2014) defined study goals and methodologies. Additional planning workshops were held before the first summer thunderstorm (March 2015), first winter haze (November 2015), and second summer (May 2016) studies.

All workshops were held at the IUM Beijing headquarters, with more than 40 invited Chinese experts from government agencies, laboratories, academia, and industry. An international advisory committee (IAC) was constituted with 10 representatives from the WMO, United States, United Kingdom, Finland, and Israel. The entire group defined research needs and barriers, and workshop reports are available from the corresponding author. This paper thus summarizes the SURF effort, carried out to better understand atmospheric interactions between urban areas and aerosols that affect summer convective processes and winter haze episodes.

From the first workshop, the overall SURF goal was identified as a better understanding of urban, terrain, convection, and aerosol interactions on both summer thunderstorm precipitation and winter haze episodes. The SURF project period is 2014–19 and has the following specific goals:

- conduct international collaborative field studies to improve understanding of urban impacts on convective weather systems and haze episodes;
- improve high-resolution (1 km) urban numerical weather and air quality forecast models for research and operational applications; and
- increase use and effectiveness of urban forecasts for social, economic, and environmental applications (e.g., for health, energy, climate change mitigation and adaptation, air quality, planning, and emergency response management).

The critical science needed to achieve these goals was identified as increased understandings of

- urban (i.e., UHI circulation, surface roughness, and building barrier) and complex terrain impacts on four-dimensional (4D) PBL structures (i.e., height, turbulence, and inversions) by analysis of mountain-valley-produced and urban-produced wind and thermal patterns;
- urban model parameterizations of PBL, building canopy, and water balance processes, as well as multiscale data assimilation for observation-rich cities;
- complex terrain, urban, and aerosol impacts and interactions on summer convective rainfall distribution, intensity, and timing (e.g., UHI-initiated vs bifurcated thunderstorms);
- long-range transport versus local (urban and complex terrain) processes and pollutant emission impacts on horizontal, PBL, and diurnal structures of aerosol concentration patterns and on the duration of regional winter haze and fog episodes;
- urban and complex terrain 4D meteorological and chemistry impacts on regional winter haze and fog episodes, including radiation and thermodynamic aerosols effects on PBL structures; and
- how to improve the performance of high-resolution urban-model-produced weather and air quality forecasts of summer precipitation and winter haze/fog episodes.

SURF FIELD STUDIES. To gain a greater understanding and improved predictions of urban summer convective precipitation and winter haze, the greater BTH region is ideal for observational studies, as it is the largest metroplex in north China and experiences both summer flooding and winter haze. SURF summer field studies thus focused on urban impacts on rainfall initialization, movement, and intensity, while winter field studies focused on aerosol (regional and local) sources, transport, and transformation processes. Three field programs were conducted, two of which focused on thunderstorms (July–August 2015 and July–September 2016) and one on haze (November 2015–January 2016).

Field sites and instrumentation. Operational meteorological data are collected every 5 min at 1,992 surface BTH-area automatic weather stations (AWSs), 348 of which are in Beijing. Twice-daily radiosondes are launched at 0800 and 2000 LST (where LST = UTC + 8 h) at NAN (Fig. 1b; all site and agency acronyms are defined in Table ES1 of the online supplement; https://doi.org/10.1175/BAMS-D-16-0178.2), with additional 1400 LST soundings during flood seasons (June–August). Surface energy balance fluxes have been observed operationally since 2012 by eddy-covariance techniques at one urban (IAP), three suburban (MIY, SHU, and WUQ), and one rural (SDZ) tower (all PBL observational sites are shown in Fig. 1). Other operational PBL sensors (Table 1) include four S-band weather radars and six X-band radars, nine wind profilers, and a GPS/Meteorology (GPS/MET) network, all supported by BMS, TMS, or Hebei Meteorological Service (HMS).

During field study periods, existing operational PBL networks were augmented; for example, the summer 2016 study (Table 1) added 5 wind profilers,

1 scanning Doppler lidar, a PBL aerosol micropulse lidar (MPL) each at the IAP tower and DAX sites, and 10 Vaisala CL51 ceilometers for cloud height and aerosol backscatter profiles. Continuous 10-Hz turbulent flux and mean meteorological data were also collected at multiple levels at two sites (the 325-m Beijing "supersite" tower and the 38-m Tianjin tower).

A van-mounted MPL aerosol lidar at DAX drove from the IAP fixed MPL site to IUM (Fig. 1b) on several days, while it circled the fourth ring road on one hazy day. During intensive observation periods (IOPs), five additional radiosondes were launched daily at NAN, and eight small-balloon soundings were taken daily at each of three sites (IUM, CHA, DAX) from 28 August to 2 September 2016 under all conditions. Photos of a selection of these instruments and sites are shown in Fig. 2.

About 250 BTH-area Environmental Protection Bureau (EPB) stations (35 in Beijing), in addition to 14 BMS stations, operationally measure hourly concentrations of surface: $PM_{2.5}$, PM_{10}, SO_2, NO_2, NO, NO_x, CO, and O_3. Special mobile lidar observations were also carried out during three 2016 winter IOPs. During fair-weather winter 2015 and winter 2016 IOPs (15 and 19, respectively), King Air aircraft flights were flown over preapproved flight paths (Fig. 1) at altitudes from 600 to 3,600 m (at 300-m intervals). The aircraft is equipped with atmospheric gas and aerosol instrumentation, including cloud images (resolution of 2.3 μm), cloud drop spectra (2–19,200 μm), aerosol spectra (0.11–3 μm), and meteorology probes (1-Hz sampling frequency) for temperature T, relative humidity (RH), and horizontal wind speed V and direction.

Datasets. The Urban Meteorological Data Sharing Platform (UMDSP) archives the 2015 and 2016 SURF datasets and includes site and instrument metadata, manufacturer-provided software, and quality-controlled (QCed) observations from the wind profilers, MPLs, Doppler lidar, flux towers, microwave radiometers, and radiosondes. Additional observation data (e.g., weather radar, aircraft, and lightning) will be added.

Golden-case SURF datasets (defined as well-documented, clear signal events) are available to research partners. The statuses of SURF PBL observational data are summarized in Table ES2 of the online supplement, and all SURF instrumentation sources, accuracies, sampling periods, data, etc., can be viewed and downloaded by the international research community through granted access to the UMDSP website (www.ium.cn/dataCenter/).

Table 1. Number of 2016 summer SURF PBL observational sites during normal operations (NO), plus additions during FS and IOP periods; AWS, GPS/MET, and soil moisture "surface" sites not included.

Instrument	NO	FS	IOP	Total
Wind profiler	9	5	0	14
Radiometer	3	0	0	3
Aerosol lidar	0	2	0	2
Doppler lidar	0	1	0	1
Flux tower	5	0	0	5
Ceilometer	10	0	0	10
Weather radar	4	0	0	4
X-band radar	6	0	0	6
GPS sounding	1	0	3	4
Mobile lidar	0	0	1	1

IOP forecasts. A daily procedure was followed by the SURF Forecast Group (SFG) to decide whether or not to call for summer 12-h IOP, with its additional rawinsonde soundings and/or mobile observations. Each day at 0830 LST during a field study period, SFG forecasters received the BMS 72-h operational synoptic forecast. They focused on evolving synoptic patterns to determine if thunderstorms were likely on the next day; if so, a tentative "go" (for the IOP) was issued.

At 1500 LST, BMS updated its 48-h forecast, and if thunderstorms still seemed likely on the next morning, SFG forecasters evaluated the latest synoptic maps and numerical weather prediction (NWP) forecasts. The models considered included the European Centre for Medium-Range Weather Forecasts (ECMWF) system and IUM urban (described below). Based on this evaluation, a final "go" or "no go" decision was made. The process resulted in a five-part daily forecast summary: previous-day weather situation; current (500 and 850 hPa) upper-level and surface charts; 36-h ECMWF forecast; 36-h IUM 3-km forecast; 24-h IUM 1-km urban forecast; and SFG IOP conclusions.

The forecast accuracy for summer 2015 and 2016 thunderstorm events (Table 2) shows that correct forecasts increased (because of the year of additional experience) from 67% for IOP days in 2015 to 74% for days in 2016. Correct forecasts predicted thunderstorm activity (or not) anywhere in the Beijing study area anytime on the given IOP day. The forecast procedure for haze IOPs is simpler, as winter haze mostly occurs under stable weather condition and

as severe episodes can last more than three days. The IUM operational WRF-Chem model provides 96-h forecasts, and if a haze event is forecast to occur within four days and to last for at least three days, a haze IOP [with Beijing Weather Modification Office (BJWMO) aircraft observations] is carried out until the event ends.

SURF MODELING. *IUM operational weather and air quality forecast system.* An Advanced Research version of WRF (WRF-ARW, version 3.5.1; Skamarock et al. 2008) is used as the IUM weather model in both operational and research modes. Its operational Rapid Refresh Multiscale Analysis and Prediction System (RMAPS) includes five offline, one-way

Fig. 2. Photographs of some SURF instrumentation: (a) 325-m tower at IAP, (b) small-balloon radiosonde at IUM, (c) GPS radiosonde at NAN, (d) X-band radar at SHU, (e) ceilometer at LIA, (f) mini-MPL at DAX, (g) wind profiler at SID, (h) mobile wind profiler at CHA, (i) wind profiler at SHA, (j) wind profiler at YAN, (k) wind profiler at GUC, (l) King Air airplane, (m) Doppler lidar and mini-MPL at IAP, and (n) mobile MPL (abbreviations are defined in Table ES1).

nested components, each with its own horizontal grid spacing (Δx). The system starts with ECMWF global forecasts (at 3-h intervals) and terminates with hourly weather and air quality forecasts. Relationships between these internal operational components, as well as the observational data used by each, are shown in the flowchart of Fig. 3 and described below:

- Nowcasting (NOW) model (Δx of 5 and 2.5 km) uses input from the Variational Doppler Radar Analysis System (VDRAS) for 6-h real-time forecasts, with ingested data from seven S-band weather radar and all AWS sites.
- Short-term (ST) model (Δx = 9 and 3 km) uses WRF data assimilation (WRFDA) and either the WRF NOAA/NCEP–Oregon State University–Air Force Research Laboratory–NOAA/Office of Hydrology land surface model (Noah; for rural grid points) or SLUCM (for urban grid points) land surface modules for operational 72-h forecasts, for which regional and local data are assimilated.
- Urban model (Δx = 1 km) for urban weather forecasts with the multilevel BEP + Building Energy Model (BEM) urban PBL modules for 24-h real-time (but not yet operational) forecasts and research studies, where BEM, BEP, and their urban land-use/land-cover (LU/LC) input data are described below and where its AWS assimilated input weather data were described above.
- Integration (IN) model combines observations into the NOW, ST, and urban model forecasts for objective 12-h forecasts, where its input [quantitative precipitation estimation (QPE)] are radar data and are calibrated by AWS rain gauge observations.
- Chemistry (CHEM) model (Δx = 9 and 3 km): for 96-h chemical forecasts from the WRF-Chem model, where its input emission (Q^*) and concentration (χ) data are discussed below.

In the operational mode, the 1-km domain 3 of the urban model (459 by 402 grid cells) is driven by its 3-km domain 2 (549 by 423 grid cells) output. The 3-km domain encompasses most of north China, while the 1-km domain covers most of the BTH area centered on Beijing (a somewhat larger area than in Fig. 1a).

Initial conditions (ICs) for the 3-km operational ST model are obtained through the WRF preprocessor ndown option and a 3D variational data assimilation (3DVAR) approach, which uses 9-km ST model outputs, with its IC and boundary conditions (BCs) from ECMWF, the National Centers for Environmental Prediction (NCEP) Global Forecast System (GFS), or China Meteorological Administration (CMA) Global and Regional Assimilation and Prediction System (GRAPES) and with the preferred order of usage of ECMWF (if available), GFS, and GRAPES (if necessary). The 3-km 72-h operational simulations have their ICs adjusted by WRFDA ingestion of S/C-band weather radar,

Table 2. Thunderstorm-occurrence forecast accuracy (in days) during 2015 and 2016 summer IOPs, with good/correct (underscored) and bad/incorrect (no underscore) forecasts (defined in text).

	Forecast			
	2015		2016	
Observed	**Yes**	**No**	**Yes**	**No**
Yes	7	8	20	9
No	4	17	7	26

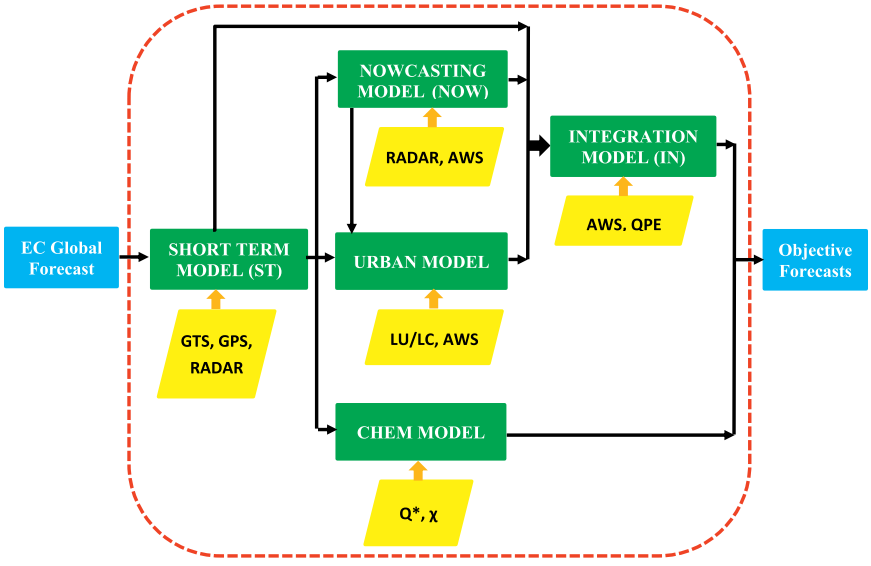

Fig. 3. IUM RMAPS modeling system flowchart, where input and output (blue boxes), component models (green boxes), and input data (yellow boxes) are discussed in the text and where EC is the ECMWF model, Q* emission inventory, and χ concentration.

Global Navigation Satellite System Zenith Total Delay (GNSS ZTD), radiosonde, Aircraft Meteorological Data Relay (AMDAR), and AWS surface observations. Then ndown provides BCs for the 1-km domain 3 urban model from its 3-km output, and VDRAS output is assimilated into the 1-km domain via four-dimensional data assimilation (FDDA).

Additional details on all of these steps are provided by Zhang et al. (2017a). RMAPS analysis and forecast products are operationally provided to BMS for weather warning and many forecasting applications (e.g., urban flooding, air pollution, weather modification, energy consumption, and emergency response management).

Application of this system for modeling SURF UHI, thunderstorm, and haze case study events are discussed below. Parameterization options for each application are also given.

Urban weather model. The 1-km WRF urban (WRF-Urban) cooling tower and 3-km thunderstorm simulations used the sophisticated multilayer urban canopy model option in WRF-Urban (Chen et al. 2011), comprising advanced versions of BEP of Martilli et al. (2002) and (in the cooling tower study) of BEM of Salamanca et al. (2010) to estimate anthropogenic heat fluxes (Q_A).

The single National Aeronautics and Space Administration (NASA) 30-m Landsat urban land-use class is scaled up to 1 or 3 km (as appropriate) and then resampled into three new urban building (i.e., low, medium, and high) classes according to gridded urban-fraction values. Required gridded urban parameters (e.g., building plan area fraction, mean building height) are derived from remotely sensed building morphological data maintained by the Beijing Institute of Surveying and Mapping and scaled up according to building plan area-weighted average [details provided in Zhang et al. (2013)].

Other WRF parameterization options selected for the two urban weather studies are listed in Table 3, where the Noah land surface model has four soil moisture and temperature layers and where the Bougeault–Lacarrere (BouLac; Bougeault and Lacarrere 1989) PBL scheme uses turbulent kinetic energy (TKE) prediction. The 9-km domain also uses Kain–Fritsch

Table 3. Models (described in text) and options (reference for each given only once) for three modeling studies reported herein; Δ*x* is horizontal grid spacing, Monin–Obukhov (MO), Monin–Obukhov–Janjić (MOJ), BEP is described in Martilli et al. (2002), and BEM is described in Salamanca et al. (2010).

	Thunderstorm-bifurcation study		Urban cooling tower study	Haze study	
	Domain 1	Domain 2	Domain 3	Domain 1	Domain 2
Models and versions	WRFDA, version 3.5.1, + WRF-Urban, version 3.5.1		WRF-Urban, version 3.5.1	WRF-Urban, version 3.3.1, + WRF-Chem, version 3.3.1	
Horizontal grid points	649 × 400	550 × 424	460 × 403	223 × 202	232 × 253
Δ*x* (km)	9	3	1	9	3
Vertical layers	50			38	
Cumulus physics	Kain–Fritsch (Kain 2004)	None	None	Grell (Grell and Dévényi 2002)	None
Microphysics	Thompson (Thompson et al. 2004)				
LW radiation	Rapid Radiative Transfer Model (RRTM; Mlawer et al. 1997)				
SW radiation	Dudhia (1989)		RRTM	Goddard (Chou and Suarez 1994)	
PBL physics	Asymmetric convective model, version 2 (ACM2; Pleim 2007)	BouLac (Bougeault and Lacarrere 1989)		Yonsei University (YSU; Hong et al. 2006)	
Rural surface	Noah (Chen and Dudhia 2001)				
Urban physics	SLUCM	BEP	BEP + BEM	SLUCM (Kusaka et al. 2001)	
Surface layer	MO	MOJ (Janjić 2002)		MO (Beljaars 1995)	
Aerosols	None			MOSAIC (Zaveri et al. 2008)	
Chemistry	None			CBMZ (Zaveri and Peters 1999)	
Photolysis	None			Fast-J scheme (Wild et al. 2000)	

(Kain 2004) cumulus parameterization, not needed in the finer-resolution domains (Fan et al. 2013).

Chemical model. The operational IUM 3-km WRF-Chem model simulates formation, transformation, and transport processes of both primary and secondary atmospheric pollutants, including gases and PM species. It used two nested grids (Table 3) with 38 vertical layers. Physical parameterizations include SLUCM; carbon bond mechanism Z (CBMZ) chemical mechanism, which includes comprehensive reactions and alterable scenarios (Zaveri et al. 1999); Model for Simulating Aerosol Interactions and Chemistry (MOSAIC) chemistry–aerosol mechanism, with its four bin sizes (Zaveri and Peters 2008); and the fast photolysis computation code of Fast-J (Wild et al. 2000).

Anthropogenic emission data for 2012, with a resolution of 0.1° × 0.1°, was developed by Multiresolution Emission Inventory for China (MEIC) group (www.meicmodel.org) and were interpolated to the 3- and 9-km model grids via a bilinear method. Meteorological ICs for the 9- and 3-km WRF-Chem model and BCs for the 9-km grid were obtained through the WRF Preprocessing System (WPS), via output from the 9-km operational ST model. An idealized vertical profile for each chemical species, based upon Northern Hemispheric, midlatitude, clean environment conditions, is used to provide chemical ICs and BCs (Earth System Research Laboratory 2017). Meteorological and chemical BCs for the 3-km model are directly obtained from the outer 9-km domain.

PRELIMINARY FINDINGS. The following preliminary results are presented only to highlight the range of SURF research activities, with additional details available in cited references and on the UMDSP website (www.ium.cn/dataCenter/).

Urban HOST. Nighttime relationships between turbulence intensity and wind speed over urban canopies were investigated to verify the hockey-stick transition (HOST) hypothesis of Sun et al. (2012, 2016), previously developed from observations over a grass field. The hypothesis describes the roles of nonlocal large coherent turbulence eddies during turbulent mixing via the linear relationship between turbulence intensity and mean wind speed V under near-neutral conditions; that is, $u_* = \sqrt{\tau/\rho}$, where τ is turbulent momentum stress, ρ is air density, and u_* is friction velocity.

Turbulent flux measurements at the 47-m level (near the urban canopy top) of the 325-m IAP tower

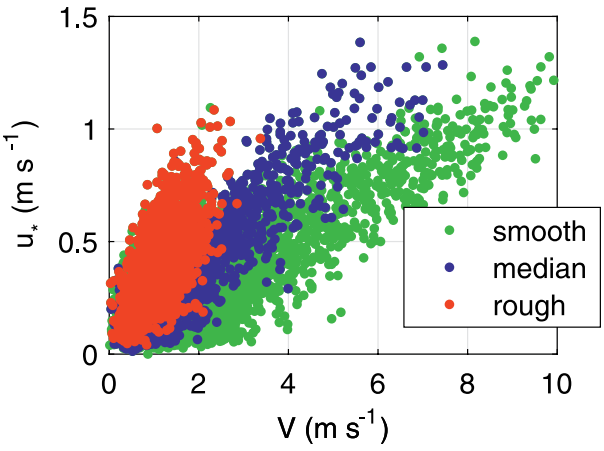

FIG. 4. Wind speed V vs friction velocity u_* (each dot represents 30-min average value) at 47-m Beijing IAP tower level on nights following sunny days in 2015 for rough, medium, and smooth surfaces (i.e., wind direction ranges of 160°–240°, 300°–360°, and 360°–160°, respectively).

(Fig. 1) were used to show that the dominant linear relationship between u_* and V also exists over urban canopies. The strong wind shear from the rough urban surfaces produces turbulence in near-neutral urban stability conditions, shown by Bornstein (1968) to exist over NYC, as stable boundary layers (BLs) over urban canopies are thus hard to maintain. The role of surface roughness on turbulent mixing is also reflected in the increasing slope (Fig. 4) of the u_*–V relationship with increasing surface roughness (sorted by wind direction) over the heterogeneous Beijing surface, consistent with the observations by Mahrt et al. (2013).

Urban surface energy balance. The exchange of energy between urban surfaces and the overlying atmosphere involves five important processes: absorption and emission of radiation by urban surfaces, turbulent transfer of heat energy to or away from the surface, evaporation of water stored in its surfaces and/or condensation of atmosphere water vapor onto the surface, thermal conduction of heat within the ground, and anthropogenic heat fluxes.

Table 4 (top) shows the average midday (1000–1400 LST) radiative and energy fluxes from both the 140-m level of the urban IAP tower and the 36-m suburban MIY tower (sites are about 50 km apart; Fig. 1) for June–August 2015. The IAP site shows slightly lower incoming shortwave radiation due to its higher atmospheric $PM_{2.5}$ concentrations (discussed below). Reflected shortwave radiation is lower at IAP, with an albedo of only 0.10, as compared to the 0.13 suburban value. Both sites have

Table 4. Midday (1000–1400 LST) average Jun–Aug 2015 mean SURF values at the 140-m level of the urban IAP and 36-m suburban MIY towers of (top) radiative and energy fluxes and (bottom) ratios of radiative and energy fluxes normalized by net or incoming radiation. Here, K is shortwave radiation; ()↓ and ()↑ are incoming and outgoing, respectively; L is longwave radiation; Q↓ is K↓ + L↓; Q_* is net all-wave radiation; Q_H and Q_E are turbulent sensible and latent heat fluxes, respectively; Q_F is IAP urban anthropogenic heat flux, calculated following Demuzere et al. (2008) and Zheng et al. (2015); heat storage ΔQ_S is $Q_* + Q_F - (Q_H + Q_E)$; Bowen ratio is Q_H/Q_E; albedo is K↑/K↓; and transmissivity τ is K↓/zenith radiation.

Mean values (W m–2)										
Site	K↓	K↑	L↓	L↑	Q↓	Q_*	Q_H	Q_E	Q_F	ΔQ_S
IAP	581.3	60.8	408.7	474.2	990.0	455.0	94.3	96.4	70.5	334.8
MIY	605.2	75.7	418.2	490.7	1,023.4	457.1	147.2	177.5	—	132.3
Ratios										
Site	**Albedo**	τ	Q_H/Q_E	Q_H/Q_*	Q_E/Q_*	$\Delta Q_S/Q_*$	Q_H/Q↓	Q_E/Q↓	$\Delta Q_S/Q$↓	
IAP	0.10	0.49	0.98	0.21	0.21	0.74	0.10	0.10	0.34	
MIY	0.13	0.51	0.83	0.32	0.39	0.29	0.14	0.17	0.13	

similar incoming longwave (LW) radiation fluxes, as its dominant control is cloudiness and its values are similar at both sites (i.e., 14 clear, 20 cloudy, and 31 rain days); the cloudiness classification procedure is described in Miao et al. (2012).

Although MIY has higher outgoing longwave radiation, the net all-wave radiations are nearly equal. Significant differences existed, however, in the surface energy partitions, as IAP has smaller turbulent sensible and latent heat fluxes and thus a larger (estimated) residual heat storage. Another contributing factor to urban heat storage is its anthropogenic heat flux source (discussed below).

Daily mean Bowen ratios [ratio of turbulent sensible to latent heat flux; Table 4 (bottom)] of 0.56 and 0.49 for IAP and MIY, respectively, are lower than previous urban and suburban estimates from sites with similar or larger fractional vegetated cover. For example, Tokyo, Japan, has a ratio of 1.77 in July with an urban vegetation percentage of 29% (Moriwaki and Kanda 2004), while the values for IAP and MIY are 21.7 and 37.0, respectively (Miao et al. 2012). The high Beijing urban latent heat flux Q_E is likely due to roadway greenbelt watering, air conditioning, and roadway sprinkling for dust control, while at suburban MIY, it is from crop irrigation (Miao and Chen 2014).

Urban PBL depth. PBL depth is important for many applications, including weather and air quality forecasts. Data from the Leosphere WindCube Doppler lidar (located near the IAP tower) were used to study PBL evolution on six days during the 2015 summer SURF campaign. A Doppler beam swinging (DBS) scan mode was used, which takes 4–5 or 2–3 s per beam scan with elevation angles of 75° or 90°, respectively.

Daytime convective boundary layer (CBL) depth was estimated by a vertical velocity variance threshold (1 m^2 s^{-2}; Barlow et al. 2011) as lidar wind profiles have shown this method as more accurate than maximum wind shear methods (Huang et al. 2017). This method, however, has limitations with nocturnal boundary layers (NBLs), so their tops are herein defined as where the variance decreases to 10% of its near-surface maximum (minus a background variance), following LeMone et al. (2014). These two methods have thus herein been combined to determine diurnal variations of SURF urban PBL depths. Results (Fig. 5) show clear diurnal patterns, with depths ranging from 270 to 1,500 m. They also show good agreement with the elevated inversion in the 1315 LST radiosonde potential temperature profile at the NAN site.

Normalized relative backscatter (NRB) data from two MPLs (in a vertical to zenith scan mode) were also used to concurrently estimate midday PBL heights on 11 August 2015 from 1250 to 1402 LST, both along a mobile route (Fig. 1b) and at a fixed site (adjacent to the urban IAP tower). As MPL instruments cannot be absolutely calibrated, small differences exist in NRB values when both were collocated (at start time of Fig. 6). Results show a fairly uniform urban CBL depth (about 1.2 km), with well-mixed conditions near the tower (Fig. 6a). While the mobile rural heights (about 0.8 km; Fig. 6b) were generally lower than the concurrent IAP urban values (as expected), they increased when the instrument passed through the urban areas. In addition, both sections show some PBL-top gravity wave activity,

and the mobile results also show two large 10-min rural convective periods.

Urban weather model development. RMAPS urban (RMAPS-Urban) forecasts suffer from overpredicted (especially nocturnal) 2-m temperatures and 10-m wind speeds. Use of the BEP scheme (also with default lookup table input parameters) did improve Beijing operational 2-m temperature and 10-m wind speed absolute biases by 4°C and 1 m s^{-1}, respectively (Barlage et al. 2016).

Despite the use of BEP, urban models still consistently overestimate 2-m temperatures because of incorrectly predicted surface energy balance terms. Beijing anthropogenic heat emissions are comparable to other major cities (e.g., NYC; Gutiérrez et al. 2015a), and megacity anthropogenic heat is partly due to air conditioning (A/C) systems. These systems release a mixture of sensible and latent heat to the environment, and in summer, 50%–80% of the heat released by evaporative-cooled A/C systems is latent energy (Sailor et al. 2007). Air conditioning heat releases in BEM, however, are assumed as 100% sensible heat (Salamanca et al. 2010), an important reason for the overpredicted 2-m urban temperatures.

To improve RMAPS-Urban performance, SURF simulations used the new evaporative cooling (EC) scheme of Gutiérrez et al. (2015a,b), developed for NYC and incorporated into the BEM urbanization option. Model evaluation of predicted temperatures and humidities used both data from eight urban AWS sites across Beijing and fluxes from the 140-m level of the IAP tower (Fig. 1b). The modeling period was 4–11 July 2015, which included dry (6–11 July) and wet (4–5 July) days.

Results show major improvement for daytime "total" sensible plus latent heat flux values (Figs. 7a and 7b), although the timing of its peak was about 2 h too late. The increased latent heat flux during the

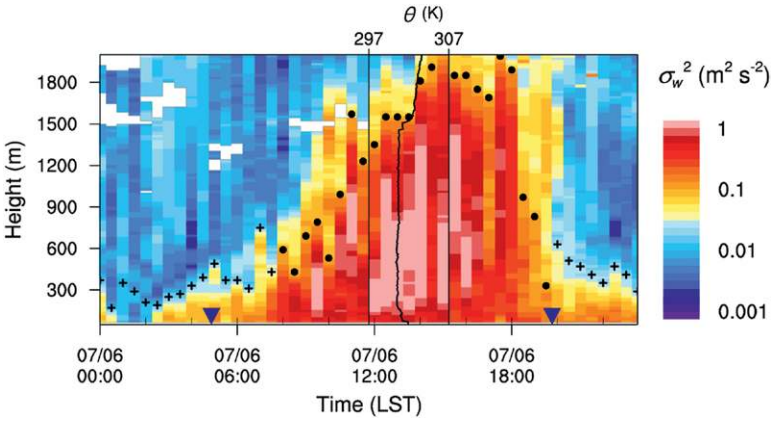

Fig. 5. DBS scans of 30-min mean vertical velocity variances (colors; m^2 s^{-2}) on 6 Jul 2015, with CBL (•) and NBL (+) depths from threshold and fractional methods, respectively (described in text); potential temperature (K) profile (solid line) from the 1315 LST NAN radiosonde; and sunrise and sunset (triangles) from Huang et al. (2017).

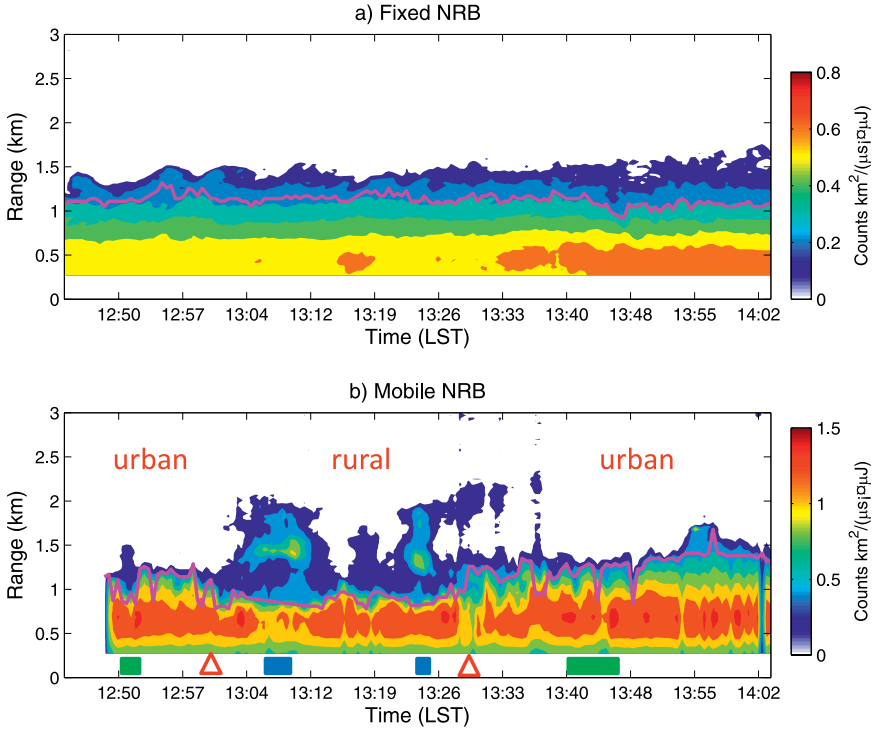

Fig. 6. Concurrent cross sections of MPL NRB (colors; note different scales) and PBL height (magenta lines) from wavelet covariance transforms on 11 Aug 2015 (a) at IAP and (b) on the mobile route of Fig. 1b, where the red triangles delineate the period in rural areas and rectangular bars indicate periods on ring roads 5 (green) and 6 (blue).

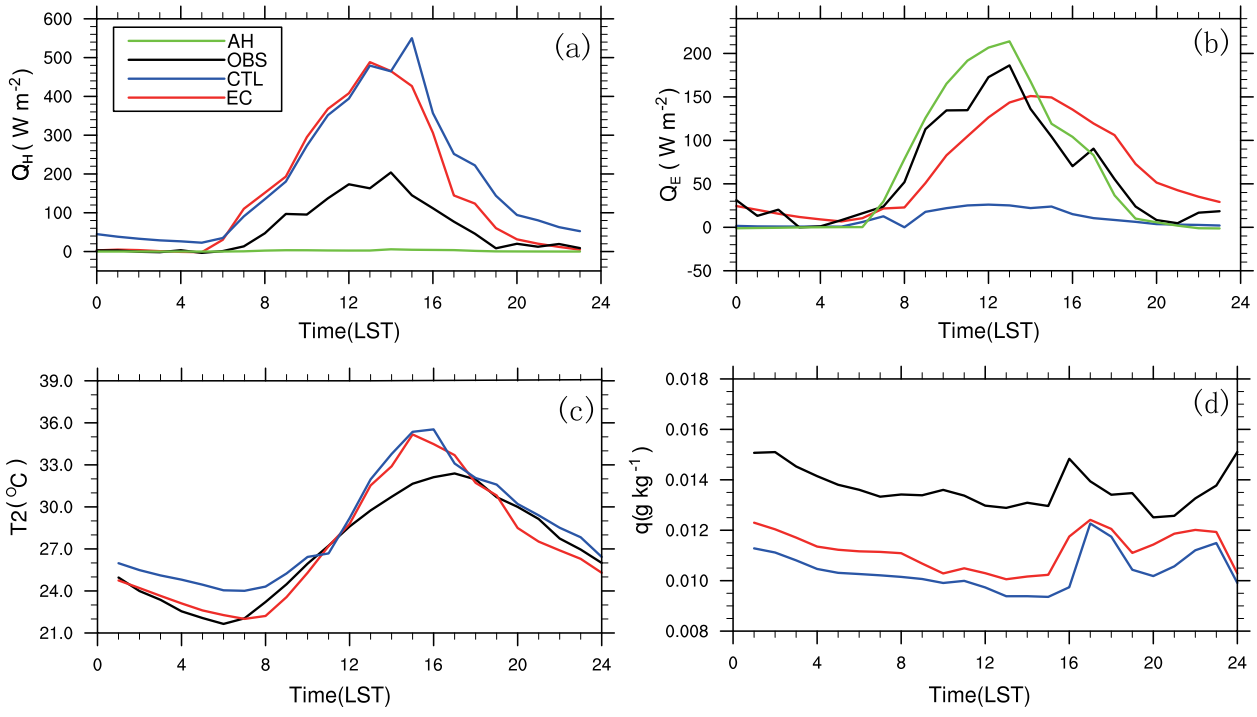

Fig. 7. Diurnal variations of average-summer observed 140-m-level IAP-tower observed (OBS; black); and WRF control (CTL; blue) and cooling tower (EC; red) simulated (a) sensible and (b) latent heat fluxes, as well as EC anthropologic heat flux component (AH; green); and 2-m average (for eight urban stations) (c) temperature and (d) specific humidity.

Table 5. Period-average (over eight urban stations) rmse and mean bias (bias) values for hourly WRF-simulated vs observed AWS 2-m temperature (*T*; °C) and specific humidity (*q*; g kg^{-1}) for dry and wet days and for the CTL and EC simulations.

	rmse		Bias	
Simulation	**CTL**	**EC**	**CTL**	**EC**
T, dry days	1.29	1.00	1.25	0.41
T, wet days	1.34	0.43	1.13	0.68
q, dry days	0.026	0.017	–0.051	0.031
q, wet days	0.035	0.024	–0.053	0.042

EC simulation (accurately) slightly increased moisture values throughout the diurnal cycle (Fig. 7d). While the corresponding decreased nighttime latent heat flux also improved the too-high temperature peak (Fig. 7c), it remained 2 h too early. The model is also much drier than the observations in the initial period, presumably because of the specified initial land surface soil moisture.

These impacts from the EC parameterization on simulated urban temperature and humidity are, however, significant (Table 5). The largest rmse improvement for temperature is for the wet days, with the reverse true for the dry days; smaller differences are seen between dry and wet days for the corresponding humidity values. The largest bias improvements with the EC formulation for both temperature and humidity, however, are on the dry days. Improvements were also seen in the PBL height and inversion structure (not shown), also consistent with the NYC results of Gutiérrez et al. (2015b). Future efforts to obtain improved urban thermal-response data will be carried out via in situ or satellite infrared observations.

Thunderstorm-bifurcation modeling. Two simulations with the 3-km IUM urban model (Table 3) were carried out for the 22 July 2015 SURF IOP thunderstorm, an a) urban case with 2010 land-use data and b) no-urban case, which converted all urban Beijing-area grid points to cropland, the dominant surface surrounding the city.

Results reproduced the weak observed UHI before the storm bifurcated around Beijing, but its magnitude was underestimated by 0.5°C (not shown). While the urban case somewhat overestimated peak precipitation and total accumulation around the city, it correctly simulated its timing, location, and bifurcation pattern (Fig. 8a vs Fig. 8c); the no-urban results

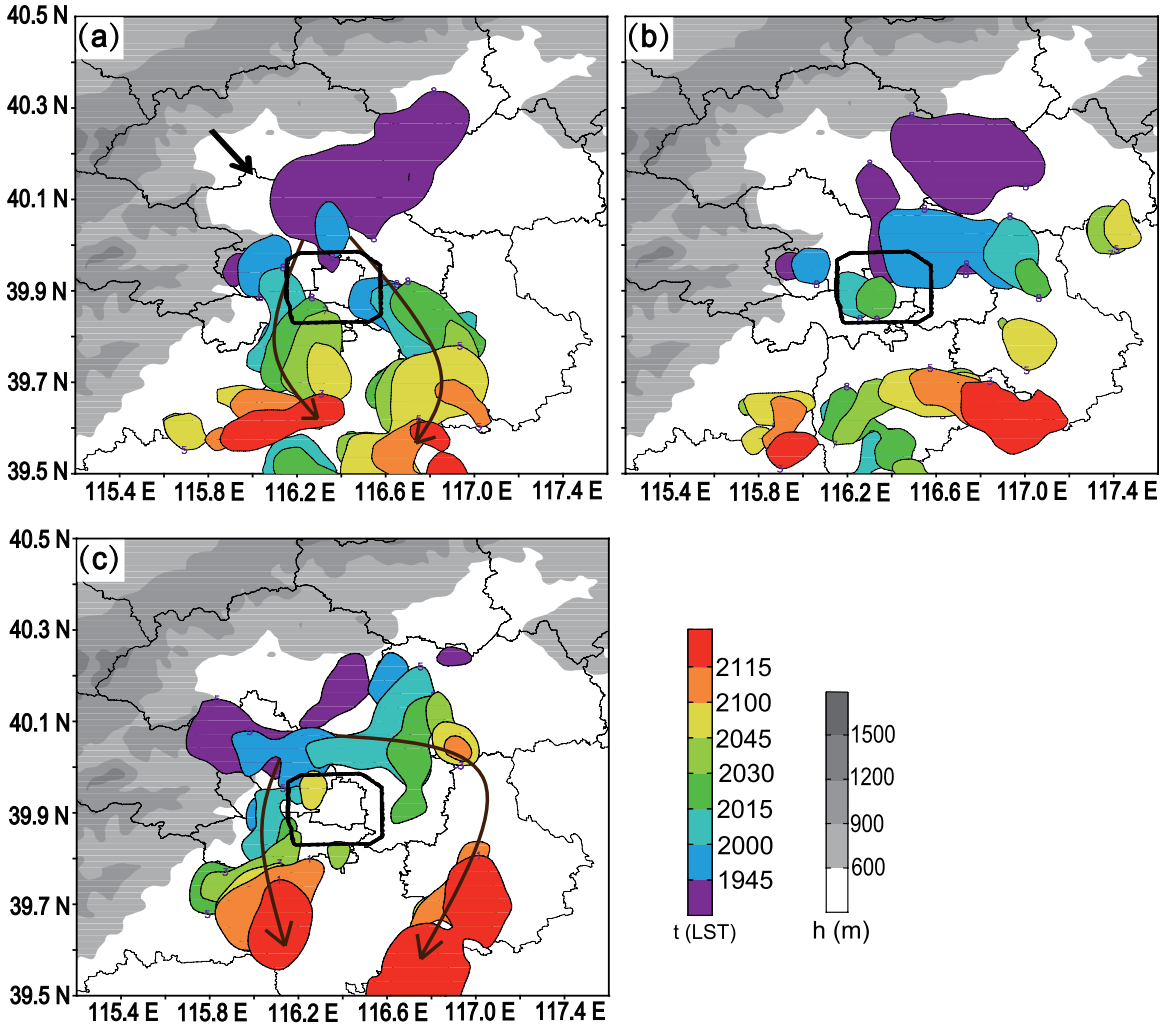

Fig. 8. Precipitation centers on 22 Jul 2015 every 15 min (colors) for the (a) urban and (b) no-urban simulations (min outline values 3–8 mm) and (c) observations (min outline values 1–5 mm), where grays are topographic height (m), black rectangle is ring road 4, short arrow is storm movement direction, and long arrows are storm-center trajectories.

(Fig. 8b) showed no bifurcation. Results were used to gain insights (not shown) into urban dynamic mechanisms leading to bifurcation [i.e., a deep (blocking) high pressure perturbation upwind of Beijing and deep downward urban vertical velocities]; additional details can be found in Dou et al. (2018, manuscript submitted to *Mon. Wea. Rev.*) and Bornstein et al. (2018, manuscript submitted to *Mon. Wea. Rev.*).

Haze event. A regional $PM_{2.5}$ haze episode occurred in the north China plain (NCP; Fig. 1a) from 26 November to 1 December 2015, when observed hourly concentrations at many Beijing sites abruptly increased and decreased several times in 24 h. Average concentrations at 35 Beijing sites (red line; Fig. 9) experienced $PM_{2.5}$ decreases at 1700 LST 29 November and 0600 LT on the next day, followed 13 h later by an increase to 500 μg m^{-3}. This value is 15 times the annual standard of 35 μg m^{-3} (no hourly standard exists in China). To understand the dynamic, physical, and chemical processes responsible for these high concentrations and rapid changes, a WRF-Chem simulation was carried out (Table 3).

The observations show that northward-moving near-surface polluted air met southward-moving clear air and thus formed a surface convergence zone. This zone first passed northward over Beijing by 2000 LST 29 November (Fig. 10a), producing high $PM_{2.5}$ values (up to 500 μg m^{-3}) over southern urban Beijing. When the cold air strengthened and pushed the boundary southward 12 h later, concentrations over the city fell abruptly to 100 μg m^{-3} (Fig. 10b). A restrengthened southerly flow then pushed the boundary northward over Beijing for a

second time at 1400 LST 30 November (Fig. 10c), and concentration in the southern part of the city thus rose to 700 μg m^{-3}. These high concentrations continued to move northward, so that 6 h later, a UHI-induced convergence (Fig. 10d) drew maximum concentrations into central Beijing from the south.

Data from the IUM Doppler lidar at the 325-m IAP tower and from the mini-MPL at HAI (7 km northwest of the tower) were also used in the analysis of $PM_{2.5}$ concentrations on 30 November. The HAI data (Fig. 11a) show increasing surface $PM_{2.5}$ starting at 0900 LST and peaking at 600 μg m^{-3} by 1700 LST. The near-surface flow from the northeast at IAP (up to 370 m) until about 0500 LST corresponds to decreasing $PM_{2.5}$ at HAI and to the low carrier-to-noise ratio (CNR) values at IAP (Fig. 11b). As the $PM_{2.5}$ front pushed into Beijing, concentrations (as reflected in the larger CNR values) steadily rose throughout the lowest 600 m of the IAP PBL. The shape of the IAP (fixed point) internal boundary layer is consistent with urban-barrier-induced surface frontal retardation of a moving cold front. As the IAP tower was always north of the concentration front (Fig. 10), winds in its lowest 200 m remained northerly, although above 300 m, they were consistently southerly.

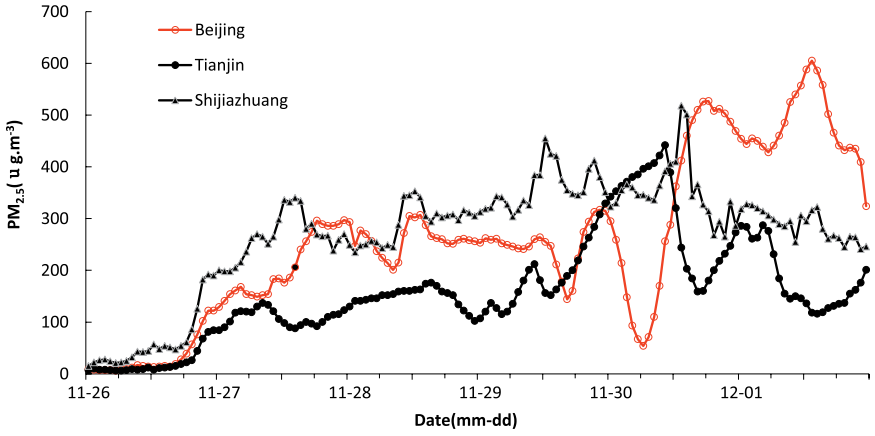

FIG. 9. Average hourly observed $PM_{2.5}$ concentration (μg m^{-3}) from 26 Nov to 1 Dec 2015 from 35 Beijing, 28 Tianjin, and 27 Shijiazhuang urban sites.

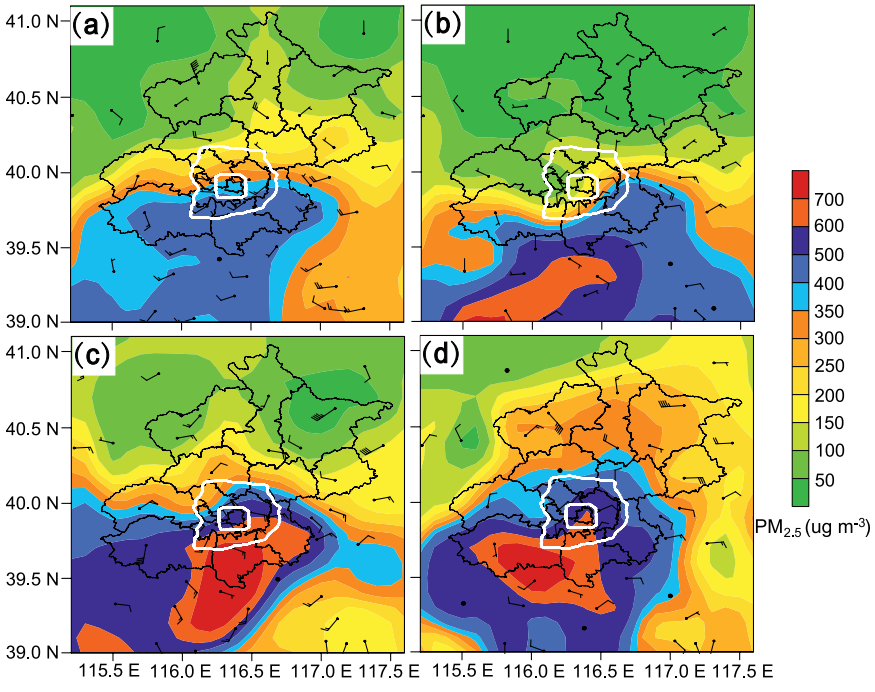

FIG. 10. Observed Beijing-area 10-m surface wind (one full barb is 1 m s^{-1}) and $PM_{2.5}$ concentration (colors; μg m^{-3}) at (a) 2000 LST 29 Nov, and (b) 0800, (c) 1400, and (d) 2000 LST 30 Nov 2015, with ring roads 4 and 6 (white circles).

Chemical modeling (Table 3) correctly simulated the maximum $PM_{2.5}$ south of Beijing at 2000 LST 29 November (Fig. 12a vs Fig. 10a) but incorrectly had the maximum southeast of the city (and not to its east) at 0800 LST 30 November (Fig. 12c vs Fig. 10c). It did, however, correctly place a narrow maximum over Beijing 12 h later (Fig. 12d vs Fig. 10d). All simulated maximum concentrations are, however, underestimated by a factor of 2. Possible reasons for this include underestimated heating-season pollutant emissions, failure to correctly simulate the complex urban meteorology conditions, and missing modeled heterologous reactions during high-humidity conditions.

Li et al. (2018) also showed that shifting wind directions (from northerly to southwesterly) above the stable boundary layer was the key process that transported the heavily polluted air over Beijing. Morning convective turbulent

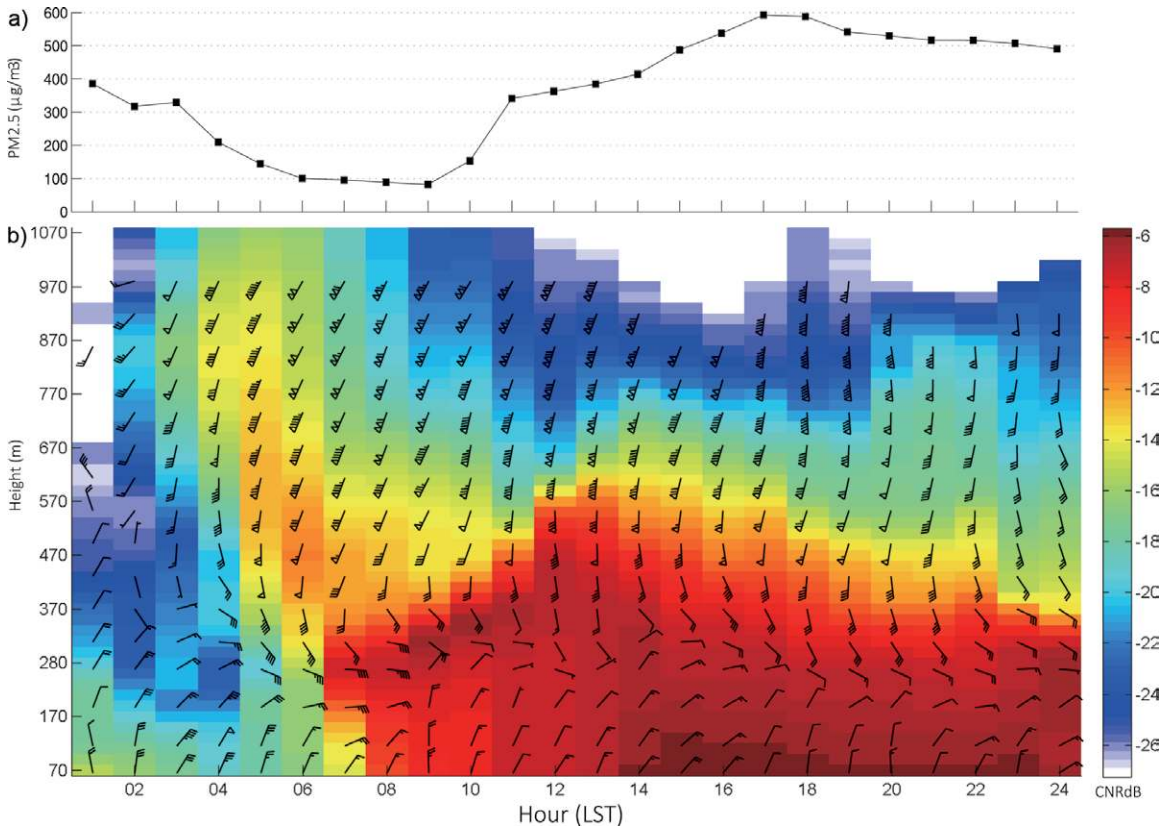

Fig. 11. Hourly observations on 30 Nov 2015 of (a) $PM_{2.5}$ concentration ($\mu g\ m^{-3}$) at HAI and (b) PBL horizontal wind vectors (one full barb is 2 m s^{-1}) and dB CNRs (colors; dB) from IAP Doppler lidar. The dB-units version of CNR used herein is CNR(dB) = $10\log_{10}$ (CNR), and as CNR(dB) is less than unity, the values in the figure are negative powers of 10.

mixing then transported upper polluted air downward, leading to the observed dramatic increases of $PM_{2.5}$ on 30 November. Such local-scale processes (e.g., dilution due to northwesterly downslope winds from the mountains around Beijing and the rapid increases of pollutants due to shifting wind directions and vertical mixing) are difficult to model and can lead to serious underestimation of $PM_{2.5}$ peak concentrations.

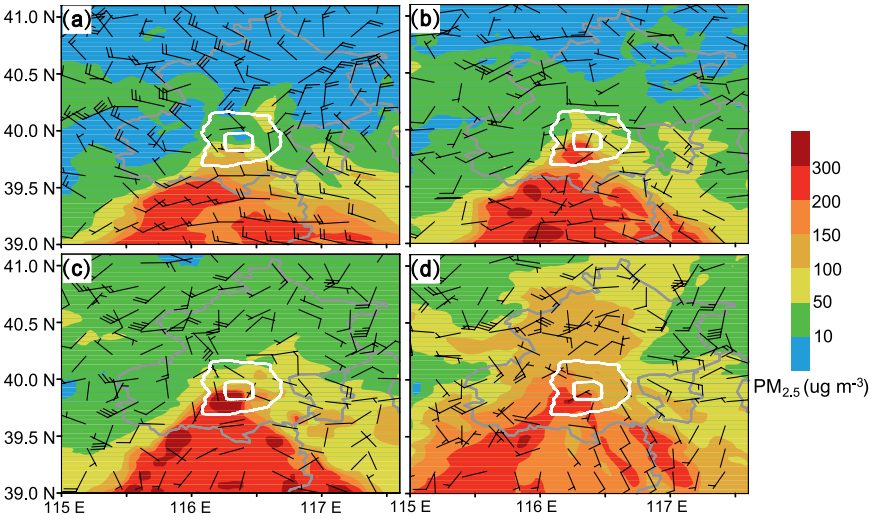

Fig. 12. Simulated Beijing-area 10-m wind (one full barb is 2 m s^{-1}) and $PM_{2.5}$ concentration (shades; $\mu g\ m^{-3}$) at (a) 2000 LST 29 Nov, and (b) 0200, (c) 0800, and (d) 2000 LST 30 Nov 2015; with ring roads 4 and 6 (white circles).

SUMMARY. SURF is truly a multidisciplinary effort, in which scientists (i.e., observationalists, modelers, meteorologists, engineers, and chemists) and forecasters collaborate across disciplines to create knowledge and to develop modeling tools to improve urban weather and air quality predictions. SURF has four components: experimental (field) studies,

numerical model development, modeled case studies of thunderstorms and haze events, and applications (improved forecasts). The structure of its lead agency (IUM), which comprises both urban PBL researchers and operational weather and air quality urban numerical forecasters, facilitates active collaboration with stakeholders, who provided useful insights for hypothesis testing and field study planning.

New scientific insights from SURF include use of flux data from a 325-m urban tower to confirm the hockey-stick transition (HOST) turbulence–wind relationships over urban canopies and a new composite diagnostic method of Doppler lidar turbulence intensities to produce more accurate estimates of diurnal variations of urban PBL depth. These new findings will be applied to reduce systemic differences between simultaneous fixed and mobile lidar observations. They will also be incorporated into IUM operational WRF Models to evaluate their roles in forecast improvement, as the IUM urbanization schemes require additional development to reduce predicted urban temperature and wind biases. A new anthropogenic cooling tower latent energy module was added to the BEM urban weather model; while it reduced model biases, additional development is also needed. Analyses of energy balance fluxes from the 325-m Beijing tower and at a nearby suburban tower showed reasonable urban-induced differences, which will also be useful in this effort.

A SURF "golden case" bifurcating summer convective thunderstorm event was analyzed and correctly simulated with the IUM urbanized WRF Model. Simulated outputs were useful in gaining insight into the bifurcation mechanisms (i.e., from deep blocking high pressure perturbations and intense downward vertical velocities); other SURF storms will be analyzed for additional insights. Regional and urban aspects of a SURF haze episode were analyzed and correctly simulated with the IUM chemical model to better understand 4D transport mechanisms. Urban land surface, anthropogenic heat, and emission impacts on such events will be further investigated.

Many challenges still need investigation within the scope of SURF, including development of advanced data assimilation methods for the dense and diverse observations at the urban scale, (e.g., aerosol PSDs). While the BEP and BEM urban parameterizations represent current state of the art for high-resolution urban forecast models, problems still exist in the partition between their latent and sensible anthropogenic heat components and in their vertical distributions. The comprehensive SURF dataset thus presents unique opportunities to test, calibrate, and develop improvements for such models, as they allow for model performance assessment, parameterization development, and golden-case analyses. An example of this is the evaporative cooling (cooling tower) SURF study, as its large errors in sensible heat flux need further investigation. Comparative studies of modeled and observational energy and radiation budgets should be carried out via model sensitivity experiments (e.g., for PBL height values).

SURF looks to explore new boundaries for high-resolution urban modeling (to subkilometer scales) for a variety of summer and winter conditions. Urban precipitation processes involve large-scale and urban forcings, as well as cloud microphysics modifications from natural and urban CCN, but aerosol impacts on urban precipitation are still largely unknown. SURF may answer some of these questions by its planned urbanization of WRF-Chem and by application of the new model to its golden-case datasets.

SURF has now entered an intensive data processing and modeling phase. These theoretical, numerical, and operational developments, as well as the massive datasets and planned journal publications, will aid future research in a wide variety of cities into the remaining unknowns of urban meteorology, climate, climate change, and air quality.

ACKNOWLEDGMENTS. SURF was funded by the Ministry of Science and Technology of China (Grant 2015DFA20870) with additional funding from the Beijing Municipal Science and Technology Commission (Grants Z151100002115045 and D171100000717003) and the National Natural Science Foundation of China (Grants 41505102, 41575010, 41605012, 41705088, and 41705090). DN acknowledges support from US NSF AGS 084742 and AGS 1522492. Without the invaluable support of the observational staffs at BMS, TMS, HMS, IAP, and the Beijing Airda Electronic Equipment Co., Ltd., the project could not have evolved.

REFERENCES

Andreae, M. O., and P. J. Crutzen, 1997: Atmospheric aerosols: Biogeochemical sources and role in atmospheric chemistry. *Science*, **276**, 1052–1058, https://doi.org/10.1126/science.276.5315.1052.

——, D. Rosenfeld, P. Artaxo, A. A. Costa, G. P. Frank, K. M. Longo, and M. A. F. Silva-Dias, 2004: Smoking rain clouds over the Amazon. *Science*, **303**, 1337–1342, https://doi.org/10.1126/science.1092779.

——, C. D. Jones, and C. P. Cox, 2005: Strong present-day aerosol cooling implies a hot future. *Nature*, **435**, 1187–1190, https://doi.org/10.1038/nature03671.

Ao, X., C. Grimmond, D. Liu, Z. Han, P. Hu, Y. Wang, X. Zhen, and J. Tan, 2016: Radiation fluxes in a business district of Shanghai, China. *J. Appl. Meteor. Climatol.*, **55**, 2451–2468, https://doi.org/10.1175/JAMC-D-16-0082.1.

Barlage, M., S. Miao, and F. Chen, 2016: Impact of physics parameterizations on high-resolution weather prediction over two Chinese megacities. *J. Geophys. Res. Atmos.*, **121**, 4487–4498, https://doi.org/10.1002/2015JD024450.

Barlow, J. F., T. M. Dunbar, E. G. Nemitz, C. R. Wood, M. W. Gallagher, F. Davies, E. O'Connor, and R. M. Harrison, 2011: Boundary layer dynamics over London, UK, as observed using Doppler lidar during REPARTEE-II. *Atmos. Chem. Phys.*, **11**, 2111–2125, https://doi.org/10.5194/acp-11-2111-2011.

Beljaars, A. C. M., 1995: The parameterization of surface fluxes in large-scale models under free convection. *Quart. J. Roy. Meteor. Soc.*, **121**, 255–270, https://doi.org/10.1002/qj.49712152203.

Bond, T. C., and Coauthors, 2013: Bounding the role of black carbon in the climate system: A scientific assessment. *J. Geophys. Res. Atmos.*, **118**, 5380–5552, https://doi.org/10.1002/jgrd.50171.

Bornstein, R. D., 1968: Observations of the urban heat island effect in New York City. *J. Appl. Meteor.*, **7**, 575–582, https://doi.org/10.1175/1520-0450(1968)007<0575:OOTUHI>2.0.CO;2.

——, 2011: Establishment of meso-met modeling case studies to evaluate the relative roles of urban dynamics and aerosols on summer thunderstorms: A proposal. *18th Conf. on Planned and Inadvertent Weather Modification and Third Symp. on Aerosol–Cloud–Climate Interactions*, Seattle, WA, Amer. Meteor. Soc., J5.2., https://ams.confex.com/ams/91Annual/recordingredirect.cgi/id/17137.

——, and G. LeRoy, 1990: Urban barrier effects on convective and frontal thunderstorms. Preprints, *Fourth Conf. on Mesoscale Processes*, Boulder, CO, Amer. Meteor. Soc., 120–121.

——, and Q. Lin, 2000: Urban heat islands and summertime convective thunderstorms in Atlanta: Three case studies. *Atmos. Environ.*, **34**, 507–516, https://doi.org/10.1016/S1352-2310(99)00374-X.

Bougeault, P., and P. Lacarrere, 1989: Parameterization of orography-induced turbulence in a mesobeta-scale model. *Mon. Wea. Rev.*, **117**, 1872–1890, https://doi.org/10.1175/1520-0493(1989)117<1872:POOITI>2.0.CO;2.

Braham, R. R., R. G. Semonin, A. H. Auer, S. A. Changnon Jr., and J. M. Hales, 1981: Summary of urban effects on clouds and rain. *METROMEX: A Review and Summary*, *Meteor. Monogr.*, No. 40, Amer. Meteor. Soc., 141–152, https://doi.org/10.1007/978-1-935704-29-4_7.

Burian, S. J., and J. M. Shepherd, 2005: Effect of urbanization on the diurnal rainfall pattern in Houston. *Hydrol. Processes*, **19**, 1089–1103, https://doi.org/10.1002/hyp.5647.

Cao, J. J., X. Tie, W. Dabberdt, Z. Z. Zhao, and T. Jie, 2013: On potential acid rain enhancement in eastern China. *J. Geophys. Res. Atmos.*, **118**, 4834–4846, https://doi.org/10.1002/jgrd.50381.

Carrió, G. G., W. R. Cotton, and W. Y. Y. Cheng, 2010: Urban growth and aerosol effects on convection over Houston. Part I: The August 2000 case. *Atmos. Res.*, **96**, 560–574, https://doi.org/10.1016/j.atmosres.2010.01.005.

Changnon, S. A., 1979: Rainfall changes in summer caused by St. Louis. *Science*, **205**, 402–404, https://doi.org/10.1126/science.205.4404.402.

——, R. G. Semonin, A. H. Auer, R. R. Braham, and J. Hales, 1981: *METROMEX: A Review and Summary. Meteor. Monogr.*, No. 40, Amer. Meteor. Soc., 81 pp.

——, R. T. Shealy, and R. W. Scott, 1991: Precipitation changes in fall, winter, and spring caused by St. Louis. *J. Appl. Meteor.*, **30**, 126–134, https://doi.org/10.1175/1520-0450(1991)030<0126:PCIFWA>2.0.CO;2.

Charlson, R. J., S. E. Schwartz, J. M. Hales, R. D. Cess, J. A. Coakley Jr., J. E. Hansen, and D. J. Hofmann, 1992: Climate forcing by anthropogenic aerosols. *Science*, **255**, 423–430, https://doi.org/10.1126/science.255.5043.423.

Chen, F., and J. Dudhia, 2001: Coupling an advanced land surface–hydrology model with the Penn State–NCAR MM5 modeling system. Part I: Model implementation. *Mon. Wea. Rev.*, **129**, 569–585, https://doi.org/10.1175/1520-0493(2001)129<0569:CAALSH>2.0.CO;2.

——, and Coauthors, 2011: The integrated WRF/urban modelling system: Development, evaluation, and applications to urban environmental problems. *Int. J. Climatol.*, **31**, 273–288, https://doi.org/10.1002/joc.2158.

Chen, W., D. Fu, S. Miao, and Y. Zhang, 2015: Impacts of aerosols from Beijing and the surrounding areas on urban precipitation (in Chinese). *Chin. Sci. Bull.*, **60**, 2124–2135, https://doi.org/10.1360/N972015-00217.

China Ministry of Environmental Protection, 2014: China Ministry of Environmental Protection issues air quality statement for important regions and 74 cities in China for 2013 (in Chinese). China Ministry of Environmental Protection, www.mep.gov.cn/gkml/hbb/qt/201403/t20140325_269648.htm.

Chou, M.-D., and M. J. Suarez, 1994: An efficient thermal infrared radiation parameterization for use in general circulation models. NASA Tech. Memo. 104606, Vol. 3, 85 pp.

Comarazamy, D. E., J. E. Gonzalez, C. A. Tepley, S. Raizada, and R. V. R. Pandya, 2006: Effects of atmospheric particle concentration on cloud microphysics over Arecibo. *J. Geophys. Res.*, **111**, D09205, https://doi.org/10.1029/2005JD006243.

Craig, K., and R. Bornstein, 2002: MM5 simulation of urban induced convective precipitation over Atlanta. Preprints, *Fourth Conf. on the Urban Environment*, Norfolk, VA, Amer. Meteor. Soc., 5–6.

Demuzere, M., K. De Ridder, and N. P. M. Van Lipzig, 2008: Modeling the energy balance in Marseille: Sensitivity to roughness length parameterizations and thermal admittance. *J. Geophys. Res.*, **113**, D16120, https://doi.org/10.1029/2007JD009113.

Di Liberto, T., 2015: India heat wave kills thousands. NOAA, www.climate.gov/news-features/event-tracker/india-heat-wave-kills-thousands.

Ding, A., and Coauthors, 2016: Long-term observation of air pollution-weather/climate interactions at the SORPES station: A review and outlook. *Front. Environ. Sci. Eng.*, **10**, 15, https://doi.org/10.1007/s11783-016-0877-3.

Dou, J., Y. Wang, R. Bornstein, and S. Miao, 2015: Observed spatial characteristics of Beijing urban climate impacts on summer thunderstorms. *J. Appl. Meteor. Climatol.*, **54**, 94–105, https://doi.org/10.1175/JAMC-D-13-0355.1.

Dudhia, J., 1989: Numerical study of convection observed during the Winter Monsoon Experiment using a mesoscale two-dimensional model. *J. Atmos. Sci.*, **46**, 3077–3107, https://doi.org/10.1175/1520-0469(1989)046<3077:NSOCOD>2.0.CO;2.

Earth System Research Laboratory, 2017: WRF-Chem user's guide. NOAA, https://ruc.noaa.gov/wrf/wrf-chem/Tutorial.html.

Fan, J., Y. Wang, D. Rosenfeld, and X. Liu, 2016: Review of aerosol–cloud interactions: Mechanisms, significance, and challenges. *J. Atmos. Sci.*, **73**, 4221–4252, https://doi.org/10.1175/JAS-D-16-0037.1.

Fan, S., H. Wang, M. Chen, and H. Gao, 2013: Study of the data assimilation of radar reflectivity with the WRF 3DVar (in Chinese). *Acta Meteor. Sin.*, **71**, 527–537.

Givati, A., and D. Rosenfeld, 2004: Quantifying precipitation suppression due to air pollution. *J. Appl. Meteor. Climatol.*, **43**, 1038–1056, https://doi.org/10.1175/1520-0450(2004)043<1038:QPSDTA>2.0.CO;2.

Grabowski, W. W., 1999: A parameterization of cloud microphysics for long-term cloud-resolving modeling of tropical convection. *Atmos. Res.*, **52**, 17–41, https://doi.org/10.1016/S0169-8095(99)00029-0.

Grell, G. A., and D. Dévényi, 2002: A generalized approach to parameterizing convection combining ensemble and data assimilation techniques. *Geophys. Res. Lett.*, **29**, 1693, https://doi.org/10.1029/2002GL015311.

Guo, S., and Coauthors, 2014: Elucidating severe urban haze formation in China. *Proc. Natl. Acad. Sci. USA*, **111**, 373–378, https://doi.org/10.1073/pnas.1419604111.

Gutiérrez, E., J. E. González, M. Arend, R. Bornstein, and A. Martilli, 2015a: Simulations of a heat wave event in New York City using a multi-layer urban parameterization. *J. Appl. Meteor. Climatol.*, **54**, 283–301, https://doi.org/10.1175/JAMC-D-14-0028.1.

——, ——, ——, ——, and ——, 2015b: On the anthropogenic heat fluxes using an air conditioning evaporative cooling parameterization for mesoscale urban canopy models. *J. Sol. Energy Eng.*, **137**, 051005, https://doi.org/10.1115/1.4030854.

Han, J. Y., J. J. Baik, and H. Lee, 2014: Urban impacts on precipitation. *Asia-Pac. J. Atmos. Sci.*, **50**, 17–30, https://doi.org/10.1007/s13143-014-0016-7.

Hong, S.-Y., Y. Noh, and J. Dudhia, 2006: A new vertical diffusion package with an explicit treatment of entrainment processes. *Mon. Wea. Rev.*, **134**, 2318–2341, https://doi.org/10.1175/MWR3199.1.

Hosannah, N., and J. E. Gonzalez, 2014: Impacts of aerosol particle size distribution and land cover land use on precipitation in a coastal urban environment using a cloud-resolving mesoscale model. *Adv. Meteor.*, **2014**, 904571, https://doi.org/10.1155/2014/904571.

Huang, M., Z. Gao, S. Miao, F. Chen, M. A. LeMone, J. Li, F. Hu, and L. Wang, 2017: Estimate of boundary-layer depths over Beijing, China, using Doppler lidar data during SURF-2015. *Bound.-Layer Meteor.*, **162**, 503–522, https://doi.org/10.1007/s10546-016-0205-2.

Huff, F. A., and J. L. Vogel, 1978: Urban, topographic and diurnal effects on rainfall in the St. Louis region. *J. Appl. Meteor.*, **17**, 565–577, https://doi.org/10.1175/1520-0450(1978)017<0565:UTADEO>2.0.CO;2.

Jacobson, M. Z., 2001: Strong radiative heating due to the mixing state of black carbon in atmospheric aerosols. *Nature*, **409**, 695–697, https://doi.org/10.1038/35055518.

Janjić, Z. I., 2002: Nonsingular implementation of the Mellor–Yamada level 2.5 scheme in the NCEP Meso model. NCEP Office Note 437, 61 pp.

Jin, M. L., and J. M. Shepherd, 2008: Aerosol relationships to warm season clouds and rainfall at

monthly scales over east China: Urban land versus ocean. *J. Geophys. Res.*, **113**, D010276, https://doi.org/10.1029/2008JD010276.

Kain, J. S., 2004: The Kain–Fritsch convective parameterization: An update. *J. Appl. Meteor.*, **43**, 170–181, https://doi.org/10.1175/1520-0450(2004)043<0170:TKCPAU>2.0.CO;2.

Kusaka, H., H. Kondo, Y. Kikegawa, and F. Kimura, 2001: A simple single-layer urban canopy model for atmospheric models: Comparison with multi-layer and slab models. *Bound.-Layer Meteor.*, **101**, 329–358, https://doi.org/10.1023/A:1019207923078.

LeMone, M. A., M. Tewari, F. Chen, and J. Dudhia, 2014: Objectively determined fair-weather NBL features in ARW-WRF and their comparison to CASES-97 observations. *Mon. Wea. Rev.*, **142**, 2709–2732, https://doi.org/10.1175/MWR-D-13-00358.1.

Li, J., J. Sun, M. Zhou, Z. Cheng, Q. Li, X. Cao, and J. Zhang, 2018: Observational analyses of dramatic developments of a severe air pollution event in the Beijing area. *Atmos. Chem. Phys.*, **18**, 3919–3935, https://doi.org/10.5194/acp-18-3919-2018.

Li, Z., F. Niu, J. Fan, Y. Liu, D. Rosenfeld, and Y. Ding, 2011: Long-term impacts of aerosols on the vertical development of clouds and precipitation. *Nat. Geosci.*, **4**, 888–889, https://doi.org/10.1038/ngeo1313.

Liu, Y. G., and P. H. Daum, 2002: Anthropogenic aerosols: Indirect warming effect from dispersion forcing. *Nature*, **419**, 580–581, https://doi.org/10.1038/419580a.

Mahrt, L., C. Thomas, S. Richardson, N. Seaman, D. Stauffer, and M. Zeeman, 2013: Non-stationary generation of weak turbulence for very stable and weak-wind conditions. *Bound.-Layer Meteor.*, **147**, 179–199, https://doi.org/10.1007/s10546-012-9782-x.

Martilli, A., A. Clappier, and M. W. Rotach, 2002: An urban surface exchange parameterization for mesoscale models. *Bound.-Layer Meteor.*, **104**, 261–304, https://doi.org/10.1023/A:1016099921195.

Miao, S., and F. Chen, 2014: Enhanced modeling of latent heat flux from urban surfaces in the Noah/single-layer urban canopy coupled model. *Sci. China Earth Sci.*, **57**, 2408–2416, https://doi.org/10.1007/s11430-014-4829-0.

——, ——, Q. Li, and S. Fan, 2011: Impacts of urban processes and urbanization on summer precipitation: A case study of heavy rainfall in Beijing on 1 August 2006. *J. Appl. Meteor. Climatol.*, **50**, 806–825, https://doi.org/10.1175/2010JAMC2513.1.

——, J. Dou, F. Chen, J. Li, and A. Li, 2012: Analysis of observations on the urban surface energy balance in Beijing. *Sci. China Earth Sci.*, **55**, 1881–1890, https://doi.org/10.1007/s11430-012-4411-6.

Mitra, C., and J. M. Shepherd, 2016. Urban precipitation: A global perspective. *Routledge Handbook of Urbanization and Global Environmental Change*, K. C. Seto, W. D. Solecki, and C. A. Griffith, Eds., Routledge, 152–168.

Mlawer, E. J., S. J. Taubman, P. D. Brown, M. J. Iacono, and S. A. Clough, 1997: Radiative transfer for inhomogeneous atmospheres: RRTM, a validated correlated-k model for the longwave. *J. Geophys. Res.*, **102**, 16 663–16 682, https://doi.org/10.1029/97JD00237.

Moriwaki, R., and M. Kanda, 2004: Seasonal and diurnal fluxes of radiation, heat, water vapor, and carbon dioxide over a suburban area. *J. Appl. Meteor.*, **43**, 1700–1710, https://doi.org/10.1175/JAM2153.1.

National Research Council, 2010: *When Weather Matters: Science and Services to Meet Critical Societal Needs.* National Academies Press, 199 pp.

Niyogi, D., P. Pyle, M. Lei, S. Aalarya, M. Kishtawal, M. Shepherd, F. Chen, and B. Wolfe, 2011: Urban modification of thunderstorms: An observational storm climatology and model case study for the Indianapolis urban region. *J. Appl. Meteor. Climatol.*, **50**, 1129–1144, https://doi.org/10.1175/2010JAMC1836.1.

Pleim, J. E., 2007: A combined local and nonlocal closure model for the atmospheric boundary layer. Part I: Model description and testing. *J. Appl. Meteor. Climatol.*, **46**, 1383–1395, https://doi.org/10.1175/JAM2539.1.

Quan, J., and Coauthors, 2013: Evolution of planetary boundary layer under different weather conditions, and its impact on aerosol concentrations. *Particuology*, **11**, 34–40, https://doi.org/10.1016/j.partic.2012.04.005.

——, Q. Liu, X. Li, Y. Gao, X. Jia, J. Sheng, and Y. Liu, 2015: Effect of heterogeneous aqueous reactions on the secondary formation of inorganic aerosols during haze events. *Atmos. Environ.*, **122**, 306–312, https://doi.org/10.1016/j.atmosenv.2015.09.068.

Robine, J.-M., S. L. Cheung, S. Le Roy, H. Van Oyen, and F. R. Herrmann, 2007: Report on excess mortality in Europe during summer 2003. EU Community Action Programme for Public Health Rep., 15 pp.

Robock, A., 1991: Surface cooling due to forest fire smoke. *J. Geophys. Res.*, **96**, 20 869–20 878, https://doi.org/10.1029/91JD02043.

Rosenfeld, D., J. Dai, X. Yu, Z. Yao, X. Xu, X. Yang, and C. Du, 2007: Inverse relations between amounts of air pollution and orographic precipitation. *Science*, **315**, 1396–1398, https://doi.org/10.1126/science.1137949.

——, U. Lohmann, G. B. Raga, C. D. O'Dowd, M. Kulmala, S. Fuzzi, A. Reissell, and M. O. Andreae,

2008: Flood or drought: How do aerosols affect precipitation? *Science*, **321**, 1309–1313, https://doi.org/10.1126/science.1160606.

Sailor, D. J., A. Brooks, M. Hart, and S. Heiple, 2007: A bottom-up approach for estimating latent and sensible heat emissions from anthropogenic sources. *Proc. Seventh Symp. on the Urban Environment*, San Diego, CA, Amer. Meteor. Soc., 3.6, https://ams.confex.com/ams/7Coastal7Urban/techprogram/paper_127290.htm.

Salamanca, F., A. Krpo, A. Martilli, and A. Clappier, 2010: A new building energy model coupled with an urban canopy parameterization for urban climate simulations—Part I. Formulation, verification, and sensitivity analysis of the model. *Theor. Appl. Climatol.*, **99**, 331–344, https://doi.org/10.1007/s00704-009-0142-9.

Shem, W., and J. M. Shepherd, 2009: On the impact of urbanization on summertime thunderstorms in Atlanta: Two numerical model case studies. *Atmos. Res.*, **92**, 172–189, https://doi.org/10.1016/j.atmosres.2008.09.013.

Shepherd, J. M., 2005: A review of current investigations of urban-induced rainfall and recommendations for the future. *Earth Interact.*, **9**, https://doi.org/10.1175/EI156.1.

——, 2013: Impacts of urbanization on precipitation and storms: Physical insights and vulnerabilities. *Climate Vulnerability: Understanding and Addressing Threats to Essential Resources*, R. A. Pielke, Ed., Elsevier, 109–125.

——, H. Pierce, and A. J. Negri, 2002: Rainfall modification by major urban areas: Observations from spaceborne rain radar on the TRMM satellite. *J. Appl. Meteor.*, **41**, 689–701, https://doi.org/10.1175/1520-0450(2002)041<0689:RMBMUA>2.0.CO;2.

Skamarock, W. C., and Coauthors, 2008: A description of the Advanced Research WRF version 3. NCAR Tech. Note NCAR/TN-475+STR, 125 pp., http://www2.mmm.ucar.edu/wrf/users/docs/arw_v3.pdf.

Stevens, B., 2008: Aerosols, Clouds, Precipitation, Climate (ACPC): Outline for a new joint IGBP/WCRP initiative. *iLEAPS Newsletter*, No. 5, iLEAPS International Project Office, University of Helsinki, Finland, 10–15, www.ileaps.org/sites/www.ileaps.org/files/iLEAPS_Newsletter_05_April_2008.pdf.

Sun, J., L. Mahrt, R. M. Banta, and Y. L. Pichugina, 2012: Turbulence regimes and turbulence intermittency in the stable boundary layer during CASES-99. *J. Atmos. Sci.*, **69**, 338–351, https://doi.org/10.1175/JAS-D-11-082.1.

——, D. H. Lenschow, M. A. LeMone, and L. Mahrt, 2016: The role of large-coherent-eddy transport in the atmospheric surface layer based on CASES-99 observations. *Bound.-Layer Meteor.*, **160**, 83–111, https://doi.org/10.1007/s10546-016-0134-0.

Tan, J., and Coauthors, 2015: Urban integrated meteorological observations: Practice and experience in Shanghai, China. *Bull. Amer. Meteor. Soc.*, **96**, 85–102, https://doi.org/10.1175/BAMS-D-13-00216.1.

Thompson, G., R. Rasmussen, and K. Manning, 2004: Explicit forecasts of winter precipitation using an improved bulk microphysics scheme. Part I: Description and sensitivity analysis. *Mon. Wea. Rev.*, **132**, 519–542, https://doi.org/10.1175/1520-0493(2004)132<0519:EFOWPU>2.0.CO;2.

Tie, X., D. Wu, and G. Brasseur, 2009: Lung cancer mortality and exposure to atmospheric aerosol particles in Guangzhou. China. *Atmos. Environ.*, **43**, 2375–2377, https://doi.org/10.1016/j.atmosenv.2009.01.036.

United Nations, 2014: World urbanization prospects: The 2014 revision—Highlights. United Nations Dept. of Economic and Social Affairs Rep. ST/ESA/SER.A/352. 27 pp.

——, 2016a: Urbanization and development: Emerging futures. United Nations Human Settlements Programme World Cities Rep. 2016, 260 pp., https://unhabitat.org/wp-content/uploads/2014/03/WCR-%20Full-Report-2016.pdf.

——, 2016b: Clear the air for children. United Nations International Children's Emergency Fund Rep. UN037345, 100 pp.

van den Heever, S. C., and W. R. Cotton, 2007: Urban aerosol impacts on downwind convective storms. *J. Appl. Meteor. Climatol.*, **46**, 828–850, https://doi.org/10.1175/JAM2492.1.

Vandentorren, S., F. Suzan, S. Medina, M. Pascal, A. Maulpoix, J.-C. Cohen, and M. Ledrans, 2004: Mortality in 13 French cities during the August 2003 heat wave. *Amer. J. Public Health*, **94**, 1518–1520, https://doi.org/10.2105/AJPH.94.9.1518.

Wang, T., and Coauthors, 2010: Air quality during the 2008 Beijing Olympics: Secondary pollutants and regional impact. *Atmos. Chem. Phys.*, **10**, 7603–7615, https://doi.org/10.5194/acp-10-7603-2010.

Wang, X., S. Miao, J. Dou, F. Dong, and J. Wang, 2016: Observation and analysis of the air pollution impacts on radiation balance of urban and suburb areas in Beijing (in Chinese). *Chin. J. Geophys.*, **59**, 3996–4006.

Wild, O., X. Zhu, and M. J. Prather, 2000: Fast-J: Accurate simulation of in- and below-cloud photolysis in tropospheric chemical models. *J. Atmos. Chem.*, **37**, 245–282, https://doi.org/10.1023/A:1006415919030.

WMO, 2013: The High Impact Weather Project (HIWeather). WMO, www.wmo.int/pages/prog/arep/wwrp/new/high_impact_weather_project.html.

Yu, M., and Y. Liu, 2015: The possible impact of urbanization on a heavy rainfall event in Beijing. *J. Geophys. Res. Atmos.*, **120**, 8132–8143, https://doi.org/10.1002/2015JD023336.

——, S. Miao, and Q. Li, 2017: Synoptic analysis and urban signatures of a heavy rainfall on 7 August 2015 in Beijing. *J. Geophys. Res. Atmos.*, **122**, 65–78, https://doi.org/10.1002/2016JD025420.

Zaveri, R. A., and L. K. Peters, 1999: A new lumped structure photochemical mechanism for large-scale applications. *J. Geophys. Res.*, **104**, 30 387–30 415, https://doi.org/10.1029/1999JD900876.

——, R. C. Easter, J. D. Fast, and L. K. Peters, 2008: Model for simulating aerosol interactions and chemistry (MOSAIC). *J. Geophys. Res.*, **113**, D13204, https://doi.org/10.1029/2007JD008782.

Zhang, Y., S. Miao, Y. Dai, and Y. Liu, 2013: Numerical simulation of characteristics of summer clear day boundary layer in Beijing and the impact of urban underlying surface on sea breeze (in Chinese). *Chin. J. Geophys.*, **56**, 2558–2573.

——, ——, and M. Chen, 2017a: Simulation experiments on high-resolution assimilation of radar thermodynamic data (in Chinese). *Acta Meteor. Sin.*, **75**, 165–177.

——, ——, Y. Dai, and R. Bornstein, 2017b: Numerical simulation of urban land surface effects on summer convective rainfall under different UHI intensity in Beijing. *J. Geophys. Res. Atmos.*, **122**, 7851–7868, https://doi.org/10.1002/2017JD026614.

Zhao, C., X. Tie, and Y. Lin, 2006: A possible positive feedback of reduction of precipitation and increase in aerosols over eastern central China. *Geophys. Res. Lett.*, **33**, L11814, https://doi.org/10.1029/2006GL025959.

Zheng Y., S. Miao, Q. Zhang, and Y. Bao, 2015: Improvements of building energy model and anthropogenic heat release from cooling system (in Chinese). *Plateau Meteor.*, **34**, 786–796, https://doi.org/10.7522/j.issn.1000-0534.2014.00035.

Zhong, S., Y. Qian, C. Zhao, R. Leung, and X. Q. Yang, 2015: A case study of urbanization impact on summer precipitation in the greater Beijing metropolitan area: Urban heat island versus aerosol effects. *J. Geophys. Res. Atmos.*, **120**, 10 903–10 914, https://doi.org/10.1002/2015JA021425.